

Formatted: Section start: Continuous

## A 1.5-Million-Year Record of Orbital and Millennial Climate Variability in the North Atlantic

David A. Hodell<sup>1</sup>, Simon J. Crowhurst<sup>1</sup>, Lucas Lourens<sup>2</sup>, Vasiliki Margari<sup>3</sup>, John Nicolson<sup>1</sup>, James E. Rolfe<sup>1</sup>, Luke C. Skinner<sup>1</sup>, Nicola Thomas<sup>1</sup>, Polychronis C. Tzedakis<sup>3</sup>, Maryline J. Mloneck-Vautravers<sup>1</sup>, Eric W. Wolff<sup>1</sup>

<sup>1</sup>Godwin Laboratory for Palaeoclimate Research, Department of Earth Sciences, University of Cambridge, Cambridge, CB2 3EQ, UK

<sup>2</sup>Department of Earth Sciences, Faculty of Geosciences, Utrecht University, Budapestlaan 4, 3584 CD Utrecht, Netherlands

<sup>3</sup>Environmental Change Research Centre, Department of Geography, University College London, London, WC1E 6BT, UK

Correspondence to: David A. Hodell (dah73@cam.ac.uk)

**Abstract.** Climate during the last glacial period was marked by abrupt instability on millennial time scales that included large swings of temperature in and around Greenland (Daansgaard-Oeschger events) and smaller, more gradual changes in Antarctica (AIM events). Less is known about the existence and nature of similar variability during older glacial periods, especially during the early Pleistocene when glacial cycles were dominantly occurring at 41-kyr intervals compared to the much longer and deeper glaciations of the more recent period. Here we report a continuous millennially-resolved record of stable isotopes of planktic and benthic foraminifera at IODP Site U1385 (the “Shackleton Site”) from the southwestern Iberian margin for the last 1.5 million years, which includes the Middle Pleistocene Transition (MPT). Our results demonstrate that millennial climate variability (MCV) was a persistent feature of glacial climate, both before and after the MPT. Prior to 1.2 Ma in the early Pleistocene, the amplitude of MCV was modulated by the 41-kyr obliquity cycle and increased when axial tilt dropped below 23.5° and benthic  $\delta^{18}\text{O}$  exceeded  $\sim 3.8\text{‰}$  (corrected to *Uvigerina*), indicating a threshold response to orbital forcing. Afterwards, MCV became focused mainly on the transitions into and out of glacial states (i.e., inceptions and terminations) and during times of intermediate ice volume. [After 1.2 Ma, obliquity continues to play a role in modulating the amplitude of MCV especially during times of glacial inceptions which are always associated with declining obliquity.](#) [A non-linear role for obliquity is also indicated by the appearance of multiples \(82, 123 kyrs\) and combination tones \(28 kyrs\) of the 41-kyr cycle.](#) [Near the end of the MPT \( \$\sim 0.65\$  Ma\), obliquity modulation of MCV amplitude wanes as quasi-periodic 100-kyr and precession power increase, coinciding with growth of oversized ice sheets on North](#)

Deleted: During the MPT (1.2-0.65 Ma), o

Deleted: bliquity continues to modulate the amplitude of MCV but in a more

Deleted: fashion

Deleted: as evidenced

Deleted: At

42 America and the appearance of Heinrich layers in North Atlantic sediments. Whereas the  
43 planktic  $\delta^{18}\text{O}$  of Site U1385 shows a strong resemblance to Greenland temperature and  
44 atmospheric methane (i.e., northern hemisphere climate), millennial changes in benthic  $\delta^{18}\text{O}$   
45 closely follow the temperature history of Antarctica for the past 800 ka. The phasing of  
46 [millennial planktic and benthic  \$\delta^{18}\text{O}\$  variation is similar to that observed for MIS 3 throughout](#)  
47 [much of the record](#), which has been suggested to mimic the signature of the bipolar seesaw --  
48 i.e., an interhemispheric asymmetry between the timing of cooling in Antarctica and warming  
49 in Greenland. The Iberian margin isotopic record suggests bipolar asymmetry was a robust  
50 feature of interhemispheric glacial climate variations for at least the past 1.5 Ma despite  
51 changing glacial boundary conditions. A strong correlation exists between millennial increases  
52 in planktic  $\delta^{18}\text{O}$  (cooling) and decreases in benthic  $\delta^{13}\text{C}$ , indicating millennial variations in  
53 North Atlantic surface temperature are mirrored by changes in deep-water circulation and  
54 remineralization of carbon in the abyssal ocean. We find strong evidence that climate  
55 variability on millennial and orbital scales are coupled across different time scales and interact,  
56 in both directions, which may be important for linking internal climate dynamics and external  
57 astronomical forcing.

**Deleted:** throughout much of the record is similar to that observed for MIS 3

## 58 59 **1. Introduction**

### 60 61 **1.1 History of Millennial Climate Variability**

62 Millennial climate variability (MCV) is operationally defined as having a recurrence time  
63 between  $10^3$  and  $10^4$  years. It excludes variation on orbital timescales but may include  
64 harmonics or combination tones of the orbital cycles that have a period of  $<10,000$  years  
65 (Berger et al., 2006). MCV is part of the background spectrum of climate variability that  
66 follows a power law connecting annual to orbital timescales (Huybers and Curry, 2006). MCV  
67 shows closer relationships to Milankovitch cycles than to higher frequency cycles or  
68 oscillations (Huybers and Curry, 2006) and some MCV may result from non-linear coupling  
69 of processes operating on orbital time scales (Hagelberg et al., 1994). Because climatic  
70 processes are intimately linked across different time scales, documenting the long-term history  
71 of MCV is important for understanding its relationship to orbitally-forced changes in  
72 Quaternary climate.

73  
74  
75 The first millennial event to be widely recognized in paleoclimate records was the Younger-  
76 Dryas when a 1,300-yr-long period of cold climate began at 12,800 yrs BP and reversed the  
77 general warming trend of the last deglaciation in the Northern Hemisphere (for a review, see

80 Mangerud, 2021). Further study of Greenland ice cores revealed the common occurrence of  
81 similar abrupt warming/cooling events during Marine Isotope Stage (MIS) 3 (~57 to 29 ka).  
82 These Dansgaard-Oeschger (D-O) events represent the rapid switching of North Atlantic  
83 climate between colder stadial and warmer interstadial states in less than 100 years with a  
84 recurrence time of ~1500 years (Dansgaard et al., 1982). The discovery of such abrupt climate  
85 changes in Greenland in the early 1980s was unexpected because of the great magnitude and  
86 rapidity of the temperature change and short recurrence times.

87  
88 Following the recognition of MCV in Greenland, the search began to see if similar events were  
89 recorded in marine sediment cores in the North Atlantic. Marine evidence for D-O events was  
90 found in variations in sediment color and the abundance of the polar foraminifer  
91 *Neogloboquadrina pachyderma* (sinistral) at DSDP Site 609 (Broecker et al., 1990; Bond et  
92 al., 1992, 1993). During some of the most extreme stadial events, North Atlantic marine  
93 sediment cores were also found to contain layers of ice-rafted detritus (IRD) that are rich in  
94 detrital carbonate derived from Paleozoic bedrock underlying Hudson Strait (Heinrich, 1988;  
95 Broecker et al., 1992; Hemming, 2004). These so-called 'Heinrich events' were attributed to  
96 massive discharges of the Laurentide Ice Sheet to the North Atlantic via Hudson Strait. The D-  
97 O cycles are packaged into longer-term cycles ("Bond cycles") where the amplitude and  
98 duration of stadial-interstadial events decrease as climate become progressively cooler until  
99 terminating in a Heinrich stadial, which is followed by a large abrupt warming (Bond et al.,  
100 1993). The recurrence time of Bond cycles and Heinrich events is on the order of every ~7-8  
101 kyrs, which is longer than D-O events.

102  
103 MCV, as expressed in Greenland temperature, has a counterpart variation in Antarctic ice cores  
104 that is smaller in magnitude and more gradual in nature than the signals found in Greenland.  
105 The one-to-one coupling between these events is often explained by changes in inter-  
106 hemispheric heat transport referred to as the thermal bipolar seesaw (Bender et al., 1994;  
107 Stocker, 1998; Blunier and Brook, 2001; EPICA Community Members, 2006; WAIS Divide  
108 Project Members, 2015). The duration of stadials in Greenland is linearly correlated with the  
109 strength of warmings in Antarctica (EPICA Community Members, 2006; WAIS Divide Project  
110 Members, 2015). The longer-duration interstadials in Antarctica (Antarctic Isotope Minimum  
111 or AIM events) are also marked by rises in atmospheric CO<sub>2</sub> (Ahn and Brook, 2014; Bauska et  
112 al., 2021), presumably from decreased stratification and increased overturning in the Southern  
113 Ocean (Anderson et al. 2009; Skinner et al., 2010, 2020). On millennial time scales, CO<sub>2</sub>

114 closely tracks Antarctic temperature with peak CO<sub>2</sub> levels lagging peak Antarctic temperature  
115 by more than 500 years (Bauska et al., 2021). The magnitude of the CO<sub>2</sub> rise is correlated with  
116 the duration of the North Atlantic stadial stage (Buizert and Schmittner, 2015), with a greater  
117 CO<sub>2</sub> response during times of prolonged stadial conditions in Greenland, such as those  
118 associated with Heinrich events. These longer-lived millennial events represent major  
119 reorganizations of the ocean-atmosphere system and have far-reaching effects well beyond the  
120 North Atlantic region.

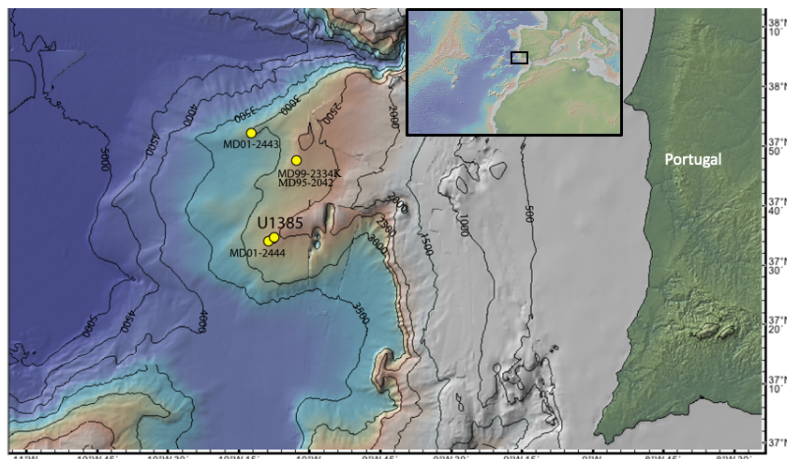
121  
122 A leading hypothesis is that changes in deep-water/ocean circulation have played a key role in  
123 MCV (for review, see McManus et al., 2004; Alley et al., 2007; Henry et al., 2016; Lynch-  
124 Stieglitz, 2017; Menviel et al., 2020). The Atlantic Meridional Overturning Circulation  
125 (AMOC) is sensitive to mode jumps that can be triggered by changes to the surface-water  
126 density in North Atlantic source areas of deep-water formation. Climate models of varying  
127 complexity have simulated millennial oscillations when forced by freshwater fluxes from  
128 melting ice (Stocker and Johnsen, 2003; Ganopolski and Rahmstorf, 2001; Timmermann et al.,  
129 2003; Rahmstorf et al., 2005), whereas others have emphasized the role of sea ice (Gildor and  
130 Tziperman, 2001; Sevellec and Fedorov, 2015; Li et al., 2005, 2010) and/or ice shelf dynamics  
131 (Dokken et al., 2013; Petersen et al., 2013). Some model simulations have shown spontaneous  
132 oscillation of the AMOC even in the absence of deliberate fresh-water forcing (Winton and  
133 Sarachik, 1993; Sakai and Peltier, 1999; de Verdière, 2007; Kleppin et al., 2015). Others have  
134 implicated orbitally-induced insolation changes or variations in atmospheric CO<sub>2</sub> as (external  
135 to the North Atlantic) triggers of MCV (Friedrich et al., 2010; Zhang et al., 2021; Yin et al.,  
136 2021; Zhang et al., 2017; Vettoretti et al., 2022).

137  
138 Oxygen isotope records of foraminifera capable of resolving orbital-scale variations are  
139 numerous (for a summary of records and resolutions, see fig. 2 of Ahn et al., 2017), but few  
140 long millennial-resolved records exist to examine the interaction between orbital and millennial  
141 components of the climate system. The study of long-term changes in MCV requires long  
142 continuous sedimentary sequences with high sedimentation rates from climatically sensitive  
143 areas of the world ocean. Some marine records of MCV exist beyond the last glacial cycle  
144 (McManus et al., 1999; Hodell et al., 2008; Oppo et al., 1998; Kawamura et al., 2017; Jouzel  
145 et al., 2007; Loulergue et al., 2008; Barker et al., 2011, 2015; Martrat et al., 2007; Margari et  
146 al., 2010; Alonso-Garcia et al., 2011; Burns et al., 2019; Gottschalk et al., 2020), but only a  
147 few extend beyond 800 ka into the early Pleistocene (Raymo et al., 1998; McIntyre et al., 2001;



148 Birner et al., 2016; Billups and Scheinwald, 2014; Hodell et al., 2008; Hodell et al., 2015;  
149 Hodell and Channell, 2016; Barker et al., 2021, 2022).

150  
151 Here we present a 1.5-million-year record of millennial variability in surface- and deep-water  
152 properties as recorded by stable isotopes of planktic and benthic foraminifera at IODP Site  
153 U1385 (the “Shackleton Site”) located off Portugal in the NE Atlantic Ocean (Fig. 1). The  
154 Iberian margin is a well-known location for sediment cores that capture orbital- and millennial-  
155 scale variations in North Atlantic climate (Shackleton et al., 2000; 2004; Martrat et al., 2007;  
156 Hodell et al., 2013, 2015). Because of its location in the eastern Atlantic at ~37°N, the region  
157 is sensitive to migrations in the Polar Front but is positioned far enough south that proxies don’t  
158 saturate under full glacial or interglacial conditions.



159  
160 **Figure 1.** Location of IODP Site U1385 and selected piston (MD95-2042, MD01-2444,  
161 MD01-2443) and kasten (MD99-2334K) cores on the Promontorio dos Principes de Avis,  
162 along the continental slope of the southwestern Iberian margin. The map was made with  
163 GeoMapApp ([www.geomapapp.org](http://www.geomapapp.org)) using bathymetry of Zitellini et al. (2009).

164  
165 The long, millennial-resolved isotope records from Site U1385 provide an opportunity to  
166 address several questions about the nature of MCV on orbital and millennial timescales. How  
167 common was MCV during older glacial periods of the Pleistocene? Does the nature (intensity,  
168 duration, pacing) of MCV change with orbital configuration or climate background state (ice  
169 volume, sea-level, ice sheet height)? What is the relationship between MCV and longer-term,  
170 orbitally-driven glacial-interglacial cycles – how do they interact? How did MCV change

171 across the Middle Pleistocene Transition (MPT) when ice sheets grew larger in size and the  
172 amplitude of glacial-interglacial cycles increased? Was the thermal bipolar seesaw mechanism  
173 active during older glacial periods of the Pleistocene? What role did millennial variability play  
174 in atmospheric CO<sub>2</sub> variations or vice-versa?

175

## 176 **1.2 The Iberian Margin Record**

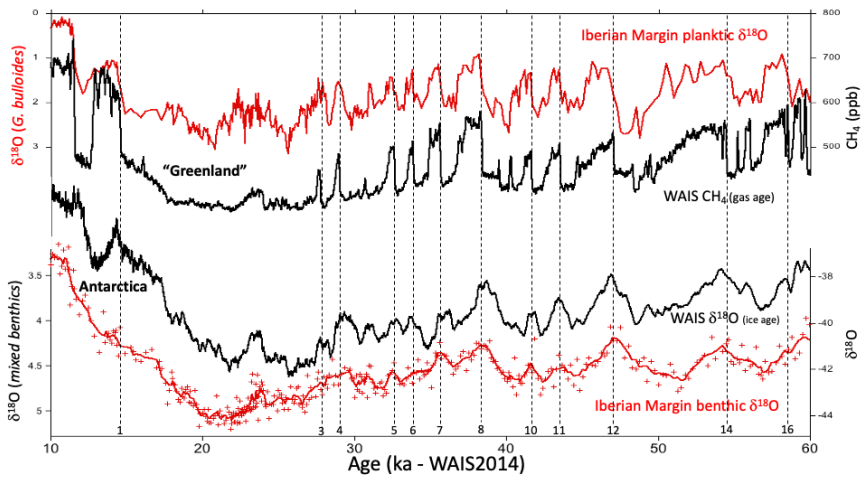
177

178 The Greenland and Antarctic ice cores provide continuous paleoclimate records to ~123,000  
179 (NGRIP Project Members, 2004) and 800,000 years (Jouzel et al., 2007) before present,  
180 respectively. Beyond the age of the oldest ice, we must rely upon rapidly accumulating marine  
181 sediments to document the older history of short-term climate variability in the North Atlantic.  
182 Piston cores from the Iberian margin off Portugal contain clear signals of D-O variability in  
183 marine sediments (Shackleton et al., 2000, 2004; Martrat et al., 2007; Margari et al., 2010,  
184 2020). High accumulation rates provide the temporal resolution needed to capture the relatively  
185 brief, abrupt temperature changes observed in the Greenland ice core. Shackleton et al. (2000,  
186 2004) demonstrated that each of the D-O events in Greenland is expressed in the Iberian margin  
187 planktic  $\delta^{18}\text{O}$  signal over the last glacial cycle (Fig. 2). In the same sediment core, the benthic  
188  $\delta^{18}\text{O}$  signal resembles the  $\delta\text{D}$  record in Antarctic ice cores (Shackleton et al., 2000, 2004),  
189 capturing each of the Antarctic Isotope Maximum (AIM) events (Jouzel et al., 2007). Because  
190 the influence of both Greenland and Antarctic millennial events is co-registered in the same  
191 sediment core, the phasing can be determined stratigraphically without the usual limitations  
192 associated with determining the absolute ages of short-lived climate events. The observed  
193 phasing of isotope signals for the last glacial cycle is consistent with the relative changes in  
194 temperature between Antarctic and Greenland deduced from the synchronization of ice core  
195 records using methane (Fig. 2) (Blunier and Brook, 2001; WAIS Divide Project Members,  
196 2015). This pattern has been interpreted as a manifestation of the thermal bipolar seesaw  
197 (Stocker and Johnsen, 2003) and can be used to recognize a similar mode of operation of the  
198 ocean-climate system in older ice cores (Loulergue et al., 2008) and Iberian margin sediment  
199 cores (Margari et al., 2010).

200

201 The benthic  $\delta^{13}\text{C}$  signal of deep cores from the Iberian margin provides a record of changes in  
202 the  $\delta^{13}\text{C}$  of deep-water dissolved inorganic carbon (DIC), which varies with changes in deep-  
203 water source areas, mixing of water masses, and oxidation of organic matter once the water  
204 mass is isolated from the surface ocean. In Iberian margin piston cores, surface cooling is  
205 associated with systematic decreases in benthic carbon isotopes, indicating concomitant

206 changes in North Atlantic surface temperature and deep-water circulation (Martrat et al., 2007).  
 207 Cooling is associated with a shoaling of the Atlantic overturning cell that results in a decreased  
 208 influence of high- $\delta^{13}\text{C}$  North Atlantic Deep Water (NADW) and an increase of southern-  
 209 sourced waters with low  $\delta^{13}\text{C}$  at abyssal depths in the North Atlantic.  
 210



211  
 212 **Figure 2.** Comparison of Iberian margin  $\delta^{18}\text{O}$  records and polar ice cores. Top panel: Planktic  
 213  $\delta^{18}\text{O}$  from core MD95-2042 (Shackleton et al., 2000) compared with  $\text{CH}_4$  from the WAIS  
 214 Divide ice core on Antarctica (WAIS Divide Project Members, 2015); Bottom panel: benthic  
 215  $\delta^{18}\text{O}$  in core MD95-2042 compared with the  $\delta^{18}\text{O}$  record of the WAIS Divide ice core (WAIS  
 216 Divide Project Members, 2015). Vertical dashed lines are drawn at the abrupt transitions from  
 217 cold stadials to warmer interstadial conditions in Greenland and are numbered at the bottom of  
 218 the figure. Note that the phasing of planktic and benthic  $\delta^{18}\text{O}$  is the same as that inferred from  
 219 the  $\text{CH}_4$  and  $\delta^{18}\text{O}$  in the WAIS Divide ice core. This pattern has been interpreted as being  
 220 indicative of a thermal bipolar seesaw.

221  
 222 Because of the relative sensitivity of surface and deep-water signals on the Iberian margin to  
 223 millennial climate change, this area was targeted by the International Ocean Discovery  
 224 Program (IODP) to extend the record beyond the oldest piston cores from the region. In 2011,  
 225 five holes were drilled at IODP Site U1385 (the “Shackleton site”) off Portugal, resulting in  
 226 the recovery of a continuous 166.5-m sequence. A composite section was constructed by  
 227 correlating elemental data measured by core scanning XRF at 1-cm resolution in all holes

228 (Hodell et al., 2015). The U1385 record extends to 1.45 Ma (MIS 47) with an average  
229 sedimentation rate of 11 cm kyr<sup>-1</sup> (Hodell et al., 2013; 2015). The record is mostly complete  
230 except for a short hiatus at Termination V that has removed part of late MIS 12 and early MIS  
231 11 (Oliviera et al., 2016).

232  
233  
234

## 2. Materials and Methods

### 2.1 IODP Site U1385 ("Shackleton site")

235  
236

237 Site U1385 is located very near the position of piston core MD01-2444 (37° 33.88' N, 10° 8.34'  
238 W, 2656 m below sea level; Fig. 1), which consists of a 27-m long sequence representing the  
239 last 194 kyr of sediment deposition. Core MD01-2444 can be precisely correlated to Site  
240 U1385 on the basis of Ca/Ti measured every 1-cm in both cores (Hodell et al., 2015), thereby  
241 providing an equivalent depth (crncd) in Site U1385 corresponding to each depth in core  
242 MD01-2444. Placing MD01-2444 on the Site U1385 depth scale corrects for the well-known  
243 effects of stretching and compression that may affect cores recovered with the jumbo Calypso  
244 coring system (Skinner and McCave, 2003). Because we did not measure stable isotopes for  
245 the upper 23 m of Site U1385 at high resolution, the isotope records presented here consist of  
246 a splice between core MD01-2444 (Vautravers & Shackleton 2006; Margari et al., 2010;  
247 Hodell et al., 2013; Tzedakis et al., 2018) and Site U1385 (this study). The U1385 record is  
248 appended to MD01-2444 at 27.45 m in the piston core which is equivalent to 26 crncd in Site  
249 U1385, corresponding to an age of ~194 kyrs.

250

251 Oxygen and carbon isotope measurements of planktic and benthic foraminifera from Site  
252 U1385 were made at an average temporal resolution of ~200 years for the last 1.45 million  
253 years (Fig. 3). The analytical methods were similar to those described by Hodell et al. (2015).  
254 For planktic foraminifera, we used the surface-dwelling species *Globigerina bulloides* from  
255 the 250 - 350  $\mu$ m size fraction. We interpret the millennial variations in planktic  $\delta^{18}\text{O}$  of *G.*  
256 *bulloides* as reflecting variations in sea surface temperature (SST) in the NE Atlantic, which is  
257 supported by the strong inverse correlation of planktic  $\delta^{18}\text{O}$  and alkenone SST data from  
258 Iberian margin cores for the past 400 ka (Martrat et al., 2007). For benthic foraminifera, we  
259 used mostly *Cibicides wuellerstorfi* and occasionally other species of *Cibicides* from the  
260 >212  $\mu$ m size fraction. In samples where specimens of *Cibicides* spp. were absent, we used  
261  $\delta^{18}\text{O}$  of *Uvigerina peregrina* or *Globobulimina affinis*. All  $\delta^{18}\text{O}$  values for each species were  
262 corrected to *Uvigerina* using the offsets suggested by Shackleton et al. (2000) -- i.e., +0.64 for

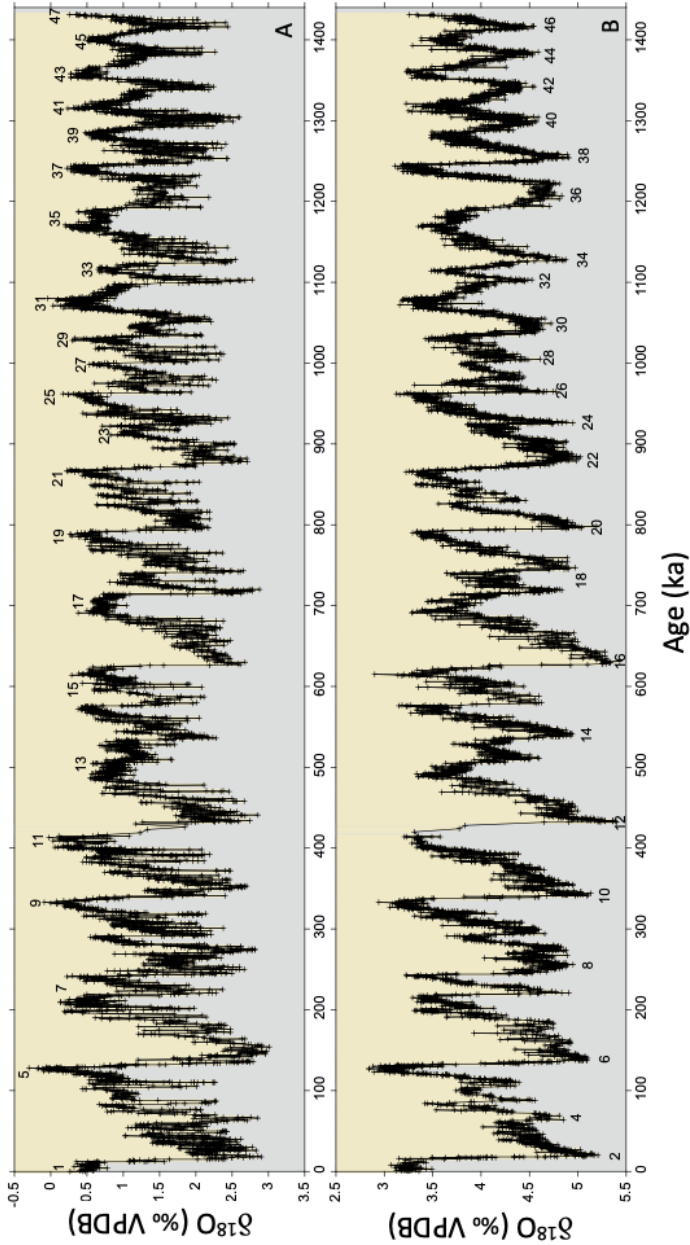


**Figure 3.** δ<sup>18</sup>O (per mil, VPDB) of the planktic foraminifer *Globigerina bulloides* (A) and mixed benthic foraminifera, mainly *Cibicoides wuellerstorfi*, corrected to *Uvigerina* (B) at IODP Site U1385. Interglacial Marine Isotope Stages (MIS) are labeled with odd-numbered interglacials in (A) and even-numbered glacial stages in (B).

263 *Cibicoides* and -0.3 for *G. affinis*. We recognise these offsets may vary slightly with time  
 264 (Hoogakker et al., 2010) but are not large enough to affect the pattern of benthic δ<sup>18</sup>O variation.

**Deleted:**

**Deleted:** benthic foraminifer *Cibicoides wuellerstorfi* (bottom) at IODP Site U1385. Interglacial Marine Isotope Stages (MIS) are labeled with odd numbers in top panel and glacial stages with even numbers in bottom panel. Photo credit: G. bulloides (<https://www.mikrotax.org/pforams/index.php?id=104034>), *C. wuellerstorfi* (<http://foraminifera.eu/single.php?no=1000394&aktion=suche>)

**Deleted:** top

268 The water depth of Site U1385 (2578 meters below sea level) places it under the influence of  
269 Northeast Atlantic Deep Water today but it was influenced by southern sourced waters during  
270 glacial periods. Variations in benthic  $\delta^{18}\text{O}$  reflect changes in temperature and the  $\delta^{18}\text{O}$  of  
271 deep water bathing the site, which was affected by ice volume on orbital time scales, albeit  
272 with such ice-volume signals being transported to the core sites on the timescale of ocean  
273 mixing (Duplessy et al., 1991; Skinner et al., 2005; Waelbroeck et al., 2011). Millennial  
274 variations in benthic  $\delta^{18}\text{O}$  are affected by changes in deep-water temperature and by the  
275 watermass endmember isotopic compositions (Shackleton et al., 2000; Skinner and  
276 Elderfield, 2003; Skinner et al., 2003, 2007). For benthic  $\delta^{13}\text{C}$ , we use only the data from the  
277 epibenthic *C. wuellerstorfi* to monitor changes in deep-water ventilation related to changes in  
278 deep ocean circulation and remineralization of organic carbon.

279  
280 Core scanning XRF measurements were made every 1 cm in piston core MD01-2444 (Hodell  
281 et al., 2013) and all holes drilled at Site U1385 (Hodell et al., 2015). The Ca/Ti signal was used  
282 to correlate among holes and define a composite spliced section consisting of intervals from  
283 Holes A, B, D and E to form a total length of 166.5 m. The spliced section used in this study  
284 consists mostly of Holes D and E with a few sections taken from Holes A and B to bridge core  
285 gaps. All sample depths are given in corrected revised meters composite depth (crmcd) that are  
286 corrected for stretching and squeezing caused by coring distortion (Pálike et al., 2005).  
287 Theoretically, the same crmcd should be equivalent in all holes but, in practice, the accuracy  
288 of the alignment among holes is dependent upon the scale of the correlative features and  
289 variability of the Ca/Ti record. We estimate that Ca/Ti features are correlated to the decimeter  
290 level or better.

291  
292 Orbital and millennial variability at Site U1385 is expressed in sediment compositional changes  
293 as reflected by elemental ratios (Hodell et al., 2013, 2015). Detrital sediment supply increases  
294 relative to biogenic production during cold periods, which is reflected in an increase in Zr/Sr  
295 and decrease in Ca/Ti (Hodell et al., 2015), which are inversely correlated with one another.  
296 During the last glacial cycle, increases in Ca/Ti occur during Greenland interstadials whereas  
297 peaks in Zr/Sr mark the stadials, particularly those containing Heinrich events (Channell et al.,  
298 2018). [Zirconium is mainly derived from zircon, which is common detrital mineral formed by  
299 magmatic and metamorphic processes or the erosion of sedimentary rocks containing zircon.  
300 Strontium is highly correlated to Ca reflecting biogenic carbonate \(CaCO<sub>3</sub>\) because of the  
301 incorporation of Sr into biogenic carbonates. We use Sr to normalize Zr, as opposed to Ca,](#)

302 [because the signals \(counts\) are similar and both are measured at the same time \(i.e., during](#)  
303 [the 30 volt scan\).](#)

Deleted: ¶

304  
305  
306  
307  
308  
309  
310

## 2.2 Chronology

311 We have updated previous age models of piston core MD01-2444 and IODP Site U1385  
312 (Hodell et al., 2013, 2015) and provide several alternative time scales so users can choose the  
313 chronology that is best suited to their specific application. The age models for MD01-2444  
314 include (0 to 194 ka): (1) WAIS Divide (WDC2014) by correlation of planktic  $\delta^{18}\text{O}$  to WAIS  
315 methane between 10 and 60 kyrs; (2) AICC 2012 for MD01-2444 by correlation of benthic  
316  $\delta^{18}\text{O}$  to  $\delta\text{D}$  of EPICA from 60 to 135 ka and using the tie points of Shin et al. (2020) from 135  
317 to 190 ka during MIS 6; (3) a Corchia speleothem chronology is provided for MIS 5 by  
318 correlation of planktic  $\delta^{18}\text{O}$  to the  $\delta^{18}\text{O}$  of the stalagmite record (Tzedakis et al., 2018).

319  
320 The age models from MD01-2444 (0 to 194 ka) are combined with those for Site U1385 (>194  
321 ka) to produce the following chronologies: (1) AICC2012 to 800 ka by iteratively correlating  
322 millennial events in Site U1385 planktic  $\delta^{18}\text{O}$  to EPICA  $\text{CH}_4$  (gas age) and benthic  $\delta^{18}\text{O}$  to  
323 EPICA  $\delta\text{D}$  (ice age), (2) Greenland Synthetic (0-800 ka) by correlation of the planktic  $\delta^{18}\text{O}$  to  
324 Barker et al. (2011), (3) revised LR04 chronology (Lisiecki and Raymo, 2005) based on  
325 correlation of Site U1385 benthic  $\delta^{18}\text{O}$  to the Prob Stack (0 to 1450 ka) (Ahn et al., 2007), and  
326 (4) an orbitally-tuned time scale by correlation of  $L^*$  to the Mediterranean sapropel stratigraphy  
327 of the eastern Mediterranean (Konijnendijk et al., 2015). In general, the tuned time scale of  
328 Site U1385 compares favorably with LR04 within the estimated error of the chronology, which  
329 is  $\pm 4$  kyr for the past million years and  $\pm 6$  kyr for the interval from 1.0 to 1.5 Ma (Lisiecki and  
330 Raymo, 2005).

331  
332 The chronology used in this paper is a hybrid model constructed using a combination of age-  
333 depth points from MD01-2444 and U1385. The age model is accurate to a precession cycle  
334 ( $\sim 23$  kyrs) but cannot provide exact absolute or relative dates for millennial events. This  
335 shortcoming limits the reliability of suborbital spectral peaks and estimation of recurrence  
336 times of millennial events. Nonetheless, the relative phasing of signals recording different

338 components of the ocean-atmosphere system can be determined stratigraphically without the  
339 need for a time scale that is accurate at suborbital resolution. This is particularly important for  
340 inferring the phase relationship between planktic and benthic  $\delta^{18}\text{O}$ , which reflects the  
341 interhemispheric leads and lags of the two polar regions.

342  
343

### 344 **3. Results**

345

#### 346 **3.1 Defining millennial variability**

347

348 To identify millennial events, it is necessary to isolate the high-frequency component of the  
349 record by eliminating the low-frequency variations related to direct orbital forcing. We  
350 experimented with several methods for accomplishing this task including high-pass filtering,  
351 Gaussian smoothing of the record followed by calculation of a residual, and subtracting the  
352 planktic and benthic  $\delta^{18}\text{O}$  values from one another. Although there are subtle differences in  
353 detection of millennial events depending on the method and thresholds used, the fundamental  
354 identification of millennial events was similar among methods. For simplicity, we settled on a  
355 high-pass Butterworth filter of second order with a cutoff frequency starting at 1/20 ky. The  
356 data were interpolated to equal time steps of 0.2 ka prior to filtering.

357

358 We identified stadial and interstadial events using the ‘findpeaks’ function in MatLab by  
359 specifying a peak height that must exceed a threshold defined by a multiplier of the standard  
360 deviation of the data (e.g.,  $1\sigma$  or  $1.5\sigma$ ), and a minimum peak duration and recurrence time (1  
361 kyr). We varied the parameters so that the algorithm correctly identifies all known D-O events  
362 for the last glacial cycle in Core MD01-2444. The same parameters are then applied to identify  
363 millennial events for the entire length of the record.

364

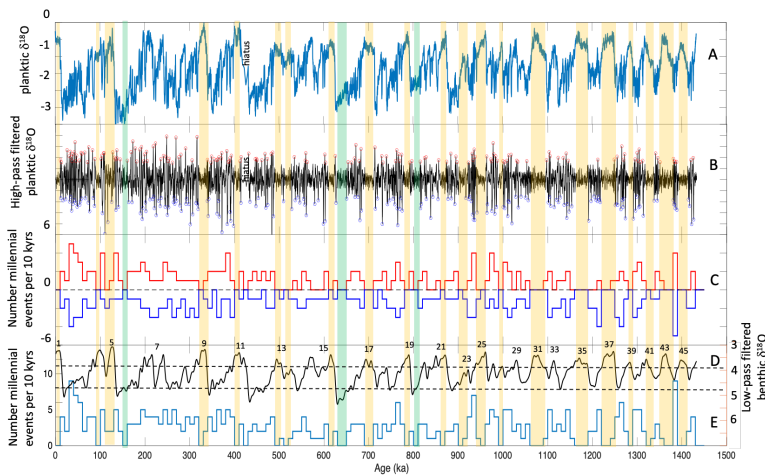
365 There is some degree of subjectivity involved in identifying millennial events. If the same event  
366 is identified in both the planktic  $\delta^{18}\text{O}$  and Zr/Sr signals (Figs. 4 and 5), we can be confident the  
367 event is robust; however, this is not always the case. Not every millennial event in planktic  
368  $\delta^{18}\text{O}$  has a corresponding change in Zr/Sr, which preferentially records the strongest of the  
369 stadial events. Additionally, the planktic  $\delta^{18}\text{O}$  record can miss stadial events associated with  
370 glacial terminations (i.e., terminal stadial event) because the decrease in the  $\delta^{18}\text{O}$  of seawater  
371 from melting ice overwhelms the  $\delta^{18}\text{O}$  increase expected from cooling. In this case, we rely on  
372 the increase in Zr/Sr to recognize the event. Most terminal stadial events are also associated  
373 with a minimum in benthic  $\delta^{13}\text{C}$  that can be used as an ancillary indicator of these events near



374 glacial terminations. Forthcoming high-resolution measurements of the alkenone SST proxy at  
375 Site U1385 will greatly improve the identification of millennial events, especially those  
376 associated with terminations (Rodrigues et al., 2017).

377  
378 We summed the number of millennial events (stadials + interstadials) over a moving non-  
379 overlapping window of 10-kyr for both planktic  $\delta^{18}\text{O}$  and Zr/Sr. Patterns of millennial  
380 variability were similar for the two proxies (Figs 4 and 5). The number of events per 10-kyr  
381 interval changes depending upon the choice of start time of the 10-kyr window and whether  
382 the analysis is run forward or backwards, but the fundamental patterns are not substantially  
383 altered. The greatest number of millennial events per 10-kyr interval occurred during MIS 3  
384 and glacial stages of the early Pleistocene from MIS 38 to 46.

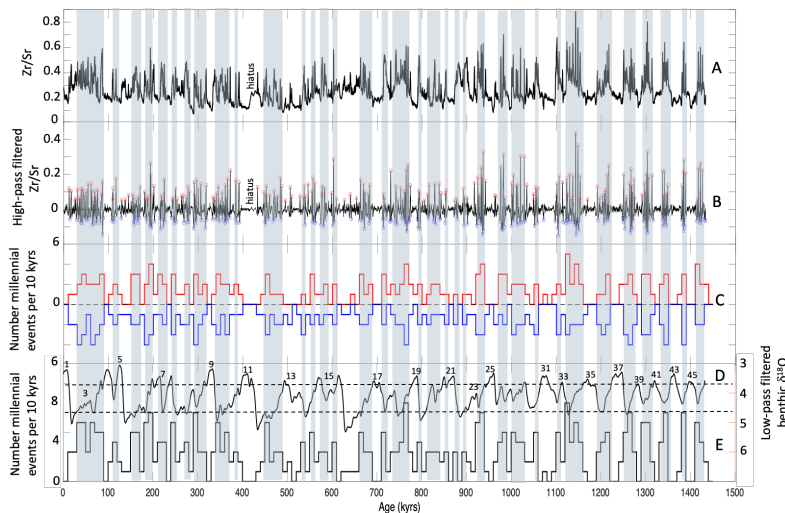
385



386  
387 **Figure 4.** (A) The  $\delta^{18}\text{O}$  record of *G. bulloides* at Site U1385. (B) High-pass filter of (A) to  
388 remove orbital frequencies and extract suborbital variability. Stadial (blue circles) and  
389 interstadial (red circles) events are identified by values that are greater than 1 standard  
390 deviation from the mean. (C) The number of stadial (blue) and interstadial (red) events in non-  
391 overlapping windows of 10,000-year duration. (D) Low-pass filter of benthic  $\delta^{18}\text{O}$  record  
392 (black) used to lookup  $\delta^{18}\text{O}$  values for each millennial event. Horizontal dashed black lines  
393 correspond to the benthic  $\delta^{18}\text{O}$  thresholds marking the window of enhanced millennial  
394 variability. (E) The number of millennial events is the sum of the stadial and interstadial events  
395 in (C). The orange shade indicates times when there are no millennial events per 10,000 years  
396 associated with full interglacial stages. Green shade indicates where there are no millennial

Formatted: Justified, None, Line spacing: 1.5 lines

397 events per 10,000 years associated with full glacial stages.



398  
399 **Figure 5.** Same as Figure 4 but for Zr/Sr. The blue shade indicates times when the total number  
400 of millennial events equals or exceeds 3 per 10,000 years, which occurs mostly during  
401 intermediate glacial states.

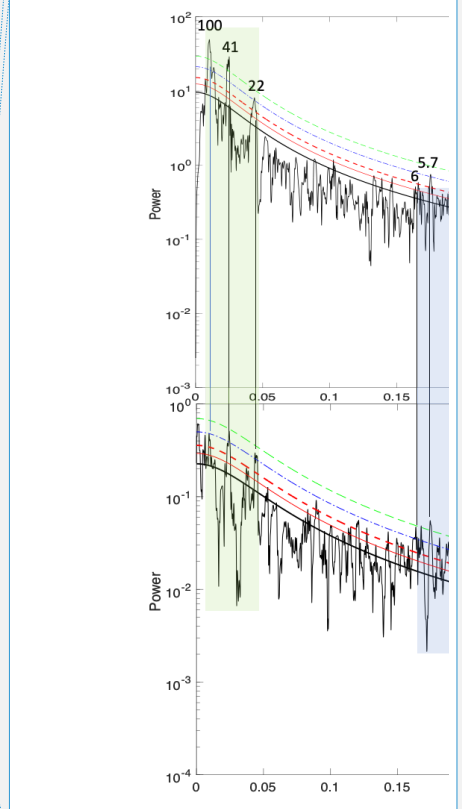
### 3.2 Description of records

402  
403  
404  
405  
406 Because it is difficult to distinguish millennial events when the Site U1385 record is plotted  
407 full scale (Fig. 3), we describe the time evolution of orbital and suborbital variability in the  
408 isotope and XRF records for the last 1.45 Ma in ~200-kyr increments: 0-200 ka (Fig. 6); 200-  
409 400 ka (Fig. 7); 400-600 ka (Fig. 8); 600-800 ka (Fig. 9); 800-1000 ka (Fig. 10); 1000-1200  
410 (Fig. 11); 1200-1450 (Fig. 12). We begin with the last 200 kyr because this is the best known  
411 period for MCV that can be used as a benchmark for comparison with MCV in the older  
412 intervals. Within each interval the record is described oldest to youngest. The records consist  
413 of planktic  $\delta^{18}\text{O}$ , benthic  $\delta^{18}\text{O}$ , benthic  $\delta^{13}\text{C}$  and Zr/Sr with stadial events identified by the gray  
414 shading. We use a modified version of the isotope nomenclature of Railsback et al. (2015) for  
415 marine isotope stages (MIS) of the last million years and the detrital layer stratigraphy of  
416 Channell et al. (2012) for Heinrich events.

418

Deleted: Page Break

Deleted: 3.2 Power Spectra



Deleted: Figure 6. Spectral analysis of planktic  $\delta^{18}\text{O}$  of *G. bulloides* (A) and Zr/Sr (B) using the multi-taper method. Significant peaks shared between the two spectra are labeled with corresponding periods in kyr. Orbital bands are

- Deleted: 1
- Deleted: 3
- Deleted: 7
- Deleted: 8
- Deleted: 9
- Deleted: 10
- Deleted: 1
- Deleted: 2
- Deleted: 3

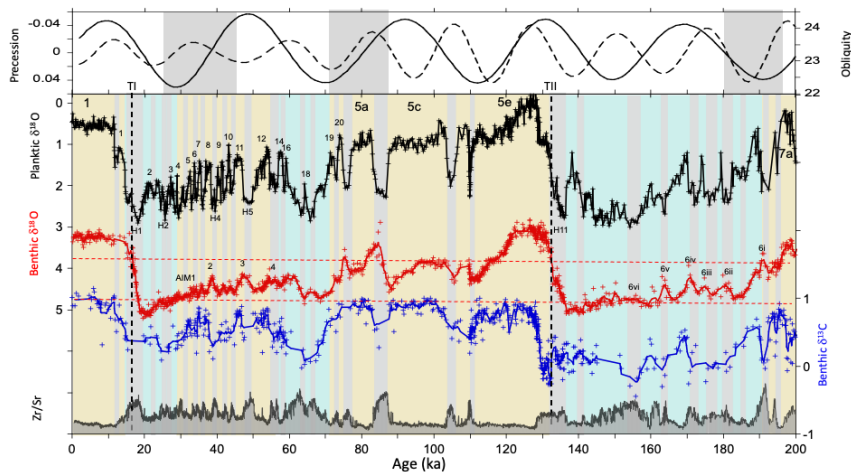
### 465 3.2.1 MIS 1-7a (0-200 ka)

466  
467 The interval from 0 to 200 ka consists mainly of the record of MD01-2444 which has been  
468 described in previous publications (Martrat et al., 2007; Margari et al., 2010, 2014; Hodell et  
469 al., 2013). MIS 6 shows a typical pattern of strong MCV at the time of glacial inception  
470 following MIS 7a (Fig. 6). Six millennial events are recognized between ~195 and 155 ka with  
471 a recurrence time ranging from 3 to 7 kyrs (Margari et al., 2010, 2014), which also correspond  
472 with carbon dioxide maxima (Shin et al., 2020). Minimum benthic  $\delta^{13}\text{C}$  values occur at ~155  
473 ka during event 6vi, which is associated with very cold alkenone SSTs (Margari et al., 2014).  
474 MCV becomes more subdued during the full glacial conditions of MIS 6 following by Heinrich  
475 stadial 11 associated with Termination II. MIS 6 shows a clear pattern of decreasing MCV  
476 during the glacial cycle with suppressed variability at the time of peak glaciation. Loulergue et  
477 al (2008) using ice core methane and Antarctic  $\delta^{18}\text{O}$  showed a similar pattern of millennial  
478 variability, with 5 interstadial events identified between 190 and 170 ka but only 1 event  
479 between 170 and 140 ka. These patterns are also reflected in marine oxygenation  
480 reconstructions from the Southern Ocean (Gottschalk et al., 2020). The close similarity in  
481 pattern between planktic  $\delta^{18}\text{O}$  and methane, and between benthic and Antarctic ice  $\delta^{18}\text{O}$ ,  
482 continues throughout the record (Wolff et al., 2022).

483  
484 Low-amplitude MCV occurs during MIS 5e (Tzedakis et al., 2018) and is followed by three  
485 strong stadial events during MIS 5d. MIS 5b is marked by a single prolonged period of stadial  
486 conditions. Millennial events DO 20 and 21, documented in the Greenland ice core, are  
487 recorded on the transition from MIS 5a to 4. MCV was relatively suppressed during MIS4  
488 except for a single event (DO 18). The last glacial cycle is unusual in that it is interrupted by a  
489 long period of strong millennial variability during MIS 3 followed by a decreased amplitude  
490 during the last glacial maximum (MIS 2) between ~27 and 19 ka (Fig. 2). MIS 2 is terminated  
491 beginning with Heinrich stadial 1 which marks the start of deglaciation. Termination I includes  
492 millennial events that occurred during the deglaciation including the Bølling-Allerød  
493 interstadial and Younger Dryas stadial.

Deleted: 3

Deleted: 7



496  
 497 **Figure 6**, 0-200 ka: Planktic  $\delta^{18}\text{O}$  of *G. bulloides* (black), benthic  $\delta^{18}\text{O}$  of *Cibicidioides spp*  
 498 (red), obliquity (solid line), precession (dashed line), benthic  $\delta^{13}\text{C}$  of *C. wuellerstorfi* (blue),  
 499 and Zr/Sr (gray). Odd marine isotope stages are numbered and shaded yellow. [Greenland](#)  
 500 [interstadials are numbered and prominent Heinrich stadials \(H\) are identified](#). Glacial periods  
 501 are shaded blue with stadial events identified by gray vertical bars. Stadials during MIS 6 are  
 502 numbered after Margari et al. (2010). Terminations are indicated by vertical dashed black lines  
 503 and roman numerals have been placed approximately near the mid-point of the deglaciation  
 504 although millennial events on the termination often make it difficult to exactly define this point.  
 505 Horizontal dashed red lines correspond to the benthic  $\delta^{18}\text{O}$  thresholds marking the window of  
 506 enhanced millennial variability. Precession and obliquity are plotted such that boreal summer  
 507 insolation increases in the up direction. The gray shading indicates times when strong MCV is  
 508 associated with declining or low obliquity, especially associated with glacial inception.

509  
 510 **3.2.2 MIS 7c-11 (200-400 ka)**

511  
 512 The transition from MIS 11 to 10 was marked by strong MCV (Fig. 7) and features in planktic  
 513 and benthic  $\delta^{18}\text{O}$  at Site U1385 can be readily correlated to the EPICA ice core records of  
 514 methane and  $\delta\text{D}$ , respectively (Nehrbass-Ahles et al., 2020). Initially, the events are paced  $\sim 5$   
 515 kyr apart from 400 to 370 ka and the recurrence time decreases to  $\sim 3$  kyrs between 365 and  
 516 355 ka. MIS 10 culminates in two prolonged Heinrich stadials (10.1 and 10.2) before  
 517 Termination IV. Low benthic  $\delta^{13}\text{C}$  values ( $< 0 \text{‰}$ ) occur at 338 and 352 ka associated with HS  
 518 10.1 and 10.2. MCV is muted during MIS 9a and 9e but relatively strong in the period between

Deleted: 7

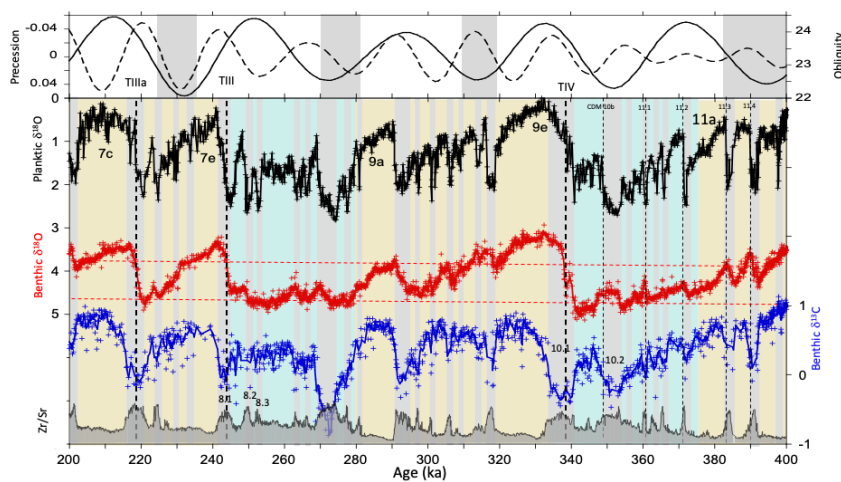
Deleted: ps

Deleted: 3

Deleted: 8

523 9a and 9e. MCV resumes during MIS 8 including three Heinrich stadial events (8.1, 8.2, 8.3)  
 524 prior to Termination III. Minimum  $\delta^{13}\text{C}$  values during MIS 8 occur at 272 ka associated with  
 525 a very strong cooling event in alkenone SST (Rodrigues et al., 2017). MCV occurs on the  
 526 transition from MIS 7e to 7d and is relatively suppressed during MIS 7c.

527  
 528  
 529



530 **Figure 7.** Same as Fig. 6, but for 200–400 ka. [Heinrich stadial 8.1, 8.2, 8.3, 10.1 and 10.1](#) are  
 531 [labelled after Channell et al. \(2012\).](#)

533  
 534  
 535

### 3.2.3 MIS 11c–15c (400–600 ka)

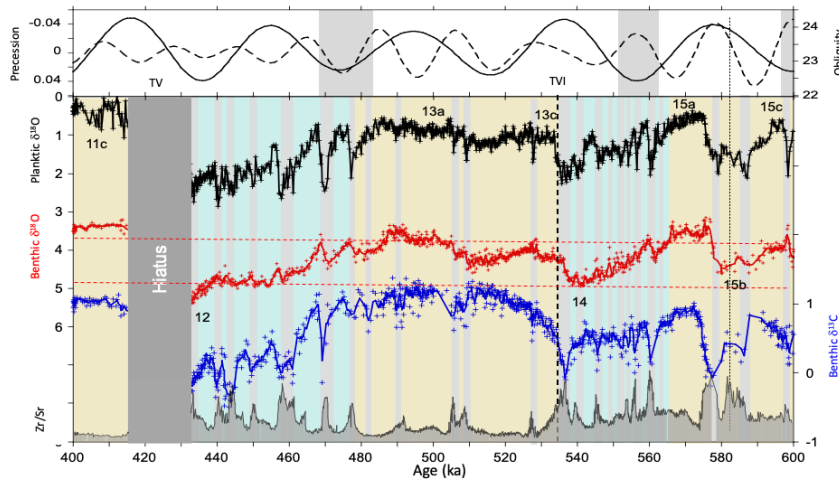
536 Both MIS 15d and 15b contain two strong stadial events, whereas MCV was suppressed during  
 537 15a, c and e (Fig. 8). MIS 14 was a relatively weak glacial by late Pleistocene standards and  
 538 MCV occurred throughout most of the glacial, and especially on the MIS 15a/14 transition.  
 539 MIS 13 shows relatively low variability with one stadial event in 13c and two near the 13b/a  
 540 transition. Strong MCV is recorded on the glacial inception of MIS 12 followed by a trend of  
 541 declining amplitude towards the peak of MIS12. A minimum in benthic  $\delta^{13}\text{C}$  values of  $<0$  ‰  
 542 occurs in the middle of MIS 12 at 455 ka. A short hiatus (~30 kyr duration) occurs at the  
 543 transition from MIS 12 to 11 that removed much of Termination V and early MIS 11.  
 544

Deleted: 8

Deleted: 7

Deleted: 3

Deleted: 9



549  
550 **Figure 8.** Same as Fig. 6 but for 400-600 ka.  
551

### 552 3.2.4 MIS 15e-20 (600-800 ka)

553  
554 The end of MIS 20 is marked by a terminal stadial event and decrease in benthic  $\delta^{13}\text{C}$  at 795  
555 ka (Fig. 9). Following MIS 19, strong MCV occurs on the MIS 19/18 transition with three  
556 distinct millennial oscillations paced at  $\sim 5$  kyr, which have been interpreted to reflect the  
557 second harmonic of precession (Ferretti et al., 2015; Sanchez-Goni et al., 2016). MIS 19 is the  
558 oldest interglacial recorded in the EPICA Dome C (EDC) ice core and three consecutive  
559 warming events (AIM) occur on the MIS 19/18 transition (Jouzel et al., 2007; Pol et al., 2010),  
560 which were also identified in the  $\text{CH}_4$  and  $\text{CO}_2$  signals (Loulergue et al., 2008; Lüthi et al.,  
561 2008). At Site U1385, the phasing between planktic and benthic  $\delta^{18}\text{O}$  variations during the  
562 MCV on the MIS19/18 transition is similar to that observed during MIS 3, suggesting an active  
563 bipolar seesaw (Fig. 2). The phasing between methane and  $\delta\text{D}$  in the EPICA ice core is difficult  
564 to determine because of large uncertainties in gas age-ice age offsets and possible diffusion in  
565 the deepest part of the ice core.

566  
567 MIS 18 consists of two distinct glaciations separated by a long interstadial period that is  
568 punctuated by a stadial event in the middle at 730 ka. Millennial variability decreases  
569 throughout the glacial inception towards the first glacial peak associated with a decrease in  
570 benthic  $\delta^{13}\text{C}$  at 742 ka. The second glacial peak of MIS 18 is marked by a very strong decrease  
571 in benthic carbon isotope values at 717 ka associated with Terminations VIII.

572

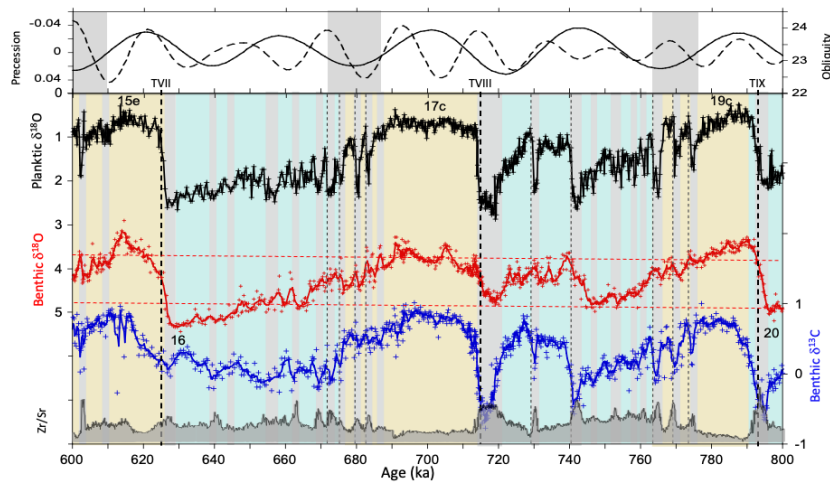
Deleted: 9

Deleted: 7

Deleted: 3

Deleted: 10

577 MIS 16 shows a trend of decreasing amplitude of MCV through the glacial cycle where the  
 578 variability is greatest on the MIS 17/16 glacial transition and diminishes towards the peak  
 579 glacial conditions of MIS 16. Strong stadial events associated with Heinrich events 16.1 and  
 580 16.2 are suspiciously absent near Termination VII, perhaps indicating the presence of a  
 581 previously undetected hiatus.



582  
 583 **Figure 9.** Same as Fig. 6 but for 600-800 ka.

584  
 585 **3.2.5 MIS 21-27 (800-1000 ka)**

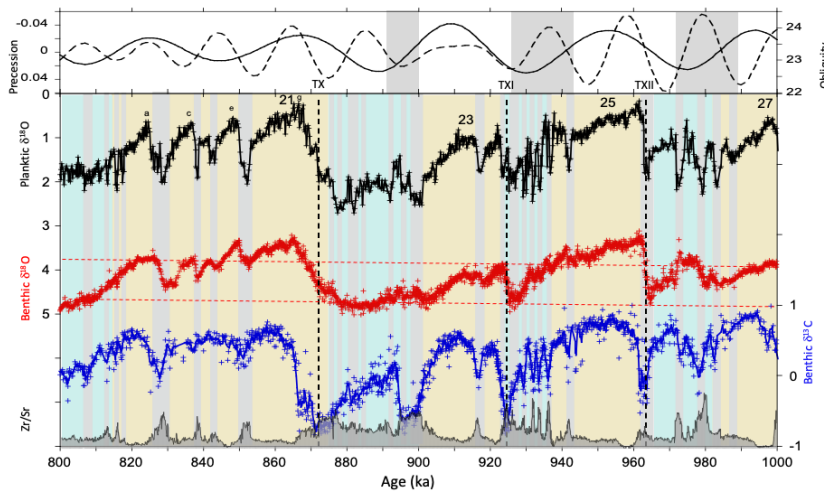
586  
 587 The pattern of increased MCV associated with the transitions from interglacial to glacial stages  
 588 continues with MIS 27/26 (Fig. 10). MIS 26 and 28 were relatively weak glacials and marked  
 589 by strong millennial variability. The interval from MIS 25-21 is often compared with MIS 5-1  
 590 because of the similarity of weak interglacial MIS 23 to MIS 3. MIS 25-21 is sometimes  
 591 erroneously described as the first '100-kyr cycle', but it consists of two obliquity cycles (Bajo  
 592 et al., 2020). The MIS 24/23 transition (TXI) was an incomplete (skipped) deglaciation, thereby  
 593 lengthening the duration of glacial conditions to ~80 kys. The pace of millennial events is faster  
 594 on the MIS25/24 transition than for some other glacial inceptions. Strong MCV is evident  
 595 throughout MIS 24 and, unlike MIS 3, MCV is relatively suppressed during MIS 23, which  
 596 contains a single strong millennial event at 919 ka. This pattern is different from the last glacial  
 597 cycle when MCV was suppressed during MIS 4 and enhanced during a significant portion of  
 598 MIS 3.

599 Glacial ice volume increased (Elderfield et al., 2012) during MIS 25-21 and major changes  
 600 occurred in deep-ocean circulation (Pena and Goldstein, 2014) and carbon cycling (Thomas

Deleted: 10  
 Deleted: 7  
 Deleted: 3  
 Deleted: 1



605 and Hodell, in press). Minimum benthic  $\delta^{13}\text{C}$  values occurred at 878, 898, and 925 ka, which  
 606 are among some of the lowest values found in the deep North Atlantic during the Quaternary  
 607 (Raymo et al., 1997; Hodell and Channell, 2016). MIS 21 has multiple substages and consists  
 608 of four warm periods that are spaced about 10 kyrs apart, which have been interpreted as the  
 609 second harmonic of precession (Ferretti et al., 2010).



610  
 611 **Figure 10.** Same as Fig. 6 but for 600-1000 ka.

612  
 613 **3.2.6 MIS 28-36 (1000-1200 ka)**

614 Although the timing of the MPT is ambiguous and dependent upon the proxy signal and method  
 615 used to define the shift in dominant period from 41 kyrs to longer periods, the length of some  
 616 of the glacial-interglacial cycles appear to increase from ~1200 ka as the shape of the benthic  
 617  $\delta^{18}\text{O}$  signal becomes less symmetrical and takes on a more sawtooth waveform (Broecker and  
 618 van Donk, 1970), reflecting a slower rate of ice sheet growth and faster rate of decay. For  
 619 example, MIS 35-34-33 has a different duration and shape than previous glacial cycles -- it is  
 620 drawn out with ~90 kyrs between TXVI and TXIV. MIS 35 was an exceptionally long  
 621 interglacial (Shackleton et al., 1990). Very strong MCV occurred on the MIS 35/34 transition  
 622 (Fig. 11), consisting of four prominent events that are paced about 5-6 kyrs apart. The abrupt  
 623 warming events that mark the start of interstadials coincide with minima in benthic  $\delta^{18}\text{O}$ ,  
 624 indicating that the phase relationship is similar to that observed during MIS 3 between  
 625 Greenland and Antarctica (Fig. 2), which is a pattern indicative of the bipolar seesaw. The  
 626

Deleted: 1  
 Deleted: 7  
 Deleted: 3

Deleted: The start of the MPT occurred at 1200 ka (Clark et al., 2006). From 1200 ka onward,  
 Deleted: and  
 Deleted: decidedly  
 Deleted: ¶  
 ¶

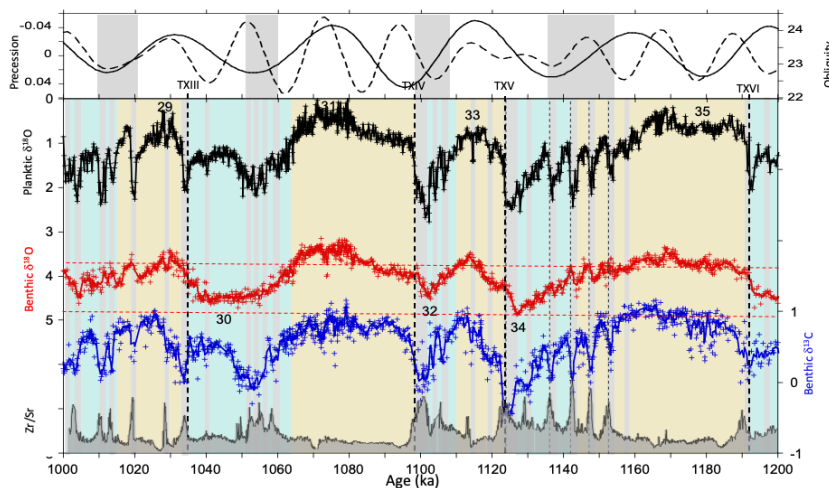
Deleted: 2



637 benthic  $\delta^{13}\text{C}$  mirrors the planktic  $\delta^{18}\text{O}$  record with strong decreases in benthic  $\delta^{13}\text{C}$  associated  
 638 with each of the stadial events.

639  
 640 The stadial events become progressively colder during MIS 34 culminating in the terminal  
 641 stadial event that occurs near the MIS 34/33 transition (TXV). This stadial is marked by a  
 642 strong decrease in benthic  $\delta^{13}\text{C}$ . Benthic  $\delta^{18}\text{O}$  begins to decrease first while planktic  $\delta^{18}\text{O}$   
 643 remains high (cold) and benthic  $\delta^{13}\text{C}$  low. This is the same phasing as observed during  
 644 Termination I on the Iberian margin when the Southern Hemisphere begins to warm at  $\sim 18$  ka  
 645 as the North Atlantic remains cold and NADW shoals (Skinner and Shackleton, 2006).

646  
 647 Millennial events occur within MIS 33 and on the glacial inception of MIS 32 with a strong  
 648 terminal stadial event associated with MIS 32/31 (TXIV). MIS 31 (1094-1062 ka) was also a  
 649 relatively long and strong interglacial (Oliveira et al., 2017). MCV occurs on the 33/32, 31/30  
 650 and 29/28 glacial inceptions and each is associated with declining obliquity.



651  
 652 **Figure 11.** Same as Fig. 6 but for 1000-1200 ka.

653  
 654 **3.2.7 MIS 37-47 (1200-1440 ka)**

655  
 656 The period from  $\sim 1250$  to 1550 ka (MIS 52) in the early Pleistocene was a time when  
 657 glacial/interglacial cycles, as recorded by benthic  $\delta^{18}\text{O}$ , were dominated by a 41-kyr period  
 658 corresponding to variations in Earth's obliquity, although precession was still significant  
 659 (Liataud et al., 2020). Similar to the last glaciation and Holocene, MCV is enhanced during  
 660 glacial periods and suppressed during interglacial stages, exhibiting a threshold response (Fig.

Deleted: 2

Deleted: 7

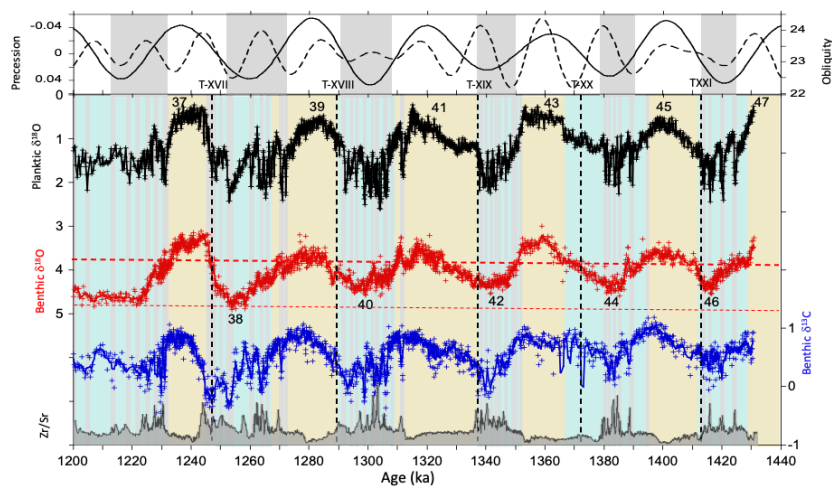
Deleted: 3

Deleted: varied dominantly at a

Deleted: coinciding with

666 12). MCV increases when obliquity drops below a threshold value of 23.5°, which corresponds  
 667 to a benthic  $\delta^{18}\text{O}$  threshold of  $\sim 3.8\text{‰}$  (corrected to *Uvigerina*). Importantly, and unlike late  
 668 Pleistocene glaciations after the MPT, MCV persists throughout most of the glacial part of the  
 669 cycle. Many of the increases in planktic  $\delta^{18}\text{O}$  (stadial events) are associated with coeval  
 670 decreases in benthic  $\delta^{13}\text{C}$  indicating a link between North Atlantic surface climate and deep-  
 671 water circulation.

Deleted: 3



672  
 673 **Figure 12.** Same as Fig. 6 but for 1200-1440 ka.  
 674

Deleted: 3

Deleted: 7

675  
 676 **4. Discussion**

677  
 678 **4.1 Millennial variability in planktic  $\delta^{18}\text{O}$**

679 Because of the great similarity between Greenland  $\delta^{18}\text{O}$  and Iberian margin planktic  $\delta^{18}\text{O}$   
 680 signals for the last glacial cycle, we interpret this proxy of surface temperature as an indicator  
 681 of MCV in the North Atlantic. XRF records of Site U1385 provided the first evidence that  
 682 MCV was a persistent feature of the climate system for at least the past 1.45 Ma (Hodell et al.,  
 683 2015), which is confirmed by comparison of the planktic  $\delta^{18}\text{O}$  and Zr/Sr signals (Figs. 4 and  
 684 5). The first-order pattern is that MCV is enhanced during glacial stages and diminished during  
 685 each of the full interglacial stages (see shading in Fig. 4), which is consistent with the relative  
 686 stability of Holocene climate relative to the last glacial period in the Greenland ice core and  
 687 with other paleoclimatic results (McManus et al., 1999; Barker et al., 2021; Sun et al., 2021;  
 688 Kawamura et al., 2017). A repeated pattern is that the end of each interglacial stage is marked  
 689

693 by the onset of strong MCV that continues through the period of glacial inception when ice  
694 sheets are expanding on North America and Eurasia. MCV associated with glacial inceptions  
695 have generally longer recurrence times than D-O events varying between 3 and 8 kyrs. A few  
696 glacial cycles of the late Pleistocene show a clear pattern of decreasing amplitude of MCV  
697 from the glacial inception towards peak glacial conditions (e.g., MIS 6, 10, 12, and 16, [Figs.](#)  
698 [6-9](#)), giving rise to a saw-tooth shape. The pattern of MCV evolves from longer stronger  
699 interstadials to shorter weaker interstadials as climate becomes progressively cooler during the  
700 glacial cycle. [In fact, it is MCV that is partly responsible for the unevenly-spaced teeth in the](#)  
701 [saw-tooth pattern of interglacial-to-glacial transitions.](#) The last glacial cycle is unusual in that  
702 the low MCV during MIS 2 and 4 is interrupted by a period of strong variability during MIS  
703 3. Such D-O-type MCV has a short recurrence time (1.5-2 kyrs) which is also found during  
704 early Pleistocene glaciations prior to 1.25 Ma (Birner et al., 2016). Almost all glacial periods  
705 end with a strong terminal stadial event that marks the start of deglaciation with some  
706 terminations containing additional millennial events during deglaciation (e.g., Bolling-Allerod  
707 and Younger Dryas oscillations).

708

#### 709 4.2 Millennial variability in benthic $\delta^{18}\text{O}$

710

711 Unlike planktic  $\delta^{18}\text{O}$ , Shackleton et al. (2000, 2004) demonstrated that variations in the benthic  
712  $\delta^{18}\text{O}$  signal of piston cores from the Iberian margin closely follows the  $\delta\text{D}$  record of Antarctic  
713 ice cores for the last glacial period (Fig. 2). The Site U1385 record indicates that this similarity  
714 extends for [at least](#) the last 800 ka (Fig. 13; [Nehrbass-Ahles et al., 2020](#)). The reason for the  
715 similarity of Iberian margin benthic  $\delta^{18}\text{O}$  and Antarctic temperature is not entirely clear  
716 (Skinner et al., 2007). Shackleton et al. (2000) originally proposed the millennial oscillations  
717 in benthic  $\delta^{18}\text{O}$  during MIS 3 reflected changes in the  $\delta^{18}\text{O}$  of seawater caused by ice volume  
718 variations of the order of 20 - 30 m of sea level equivalence (Siddall et al., 2008). An alternative  
719 explanation is that millennial variations in benthic  $\delta^{18}\text{O}$  reflect temperature changes of deep-  
720 water. In this case, the large variations in Antarctic air temperatures are damped by the thermal  
721 mass of the deep ocean and translate into small changes in benthic  $\delta^{18}\text{O}$ , reflecting temperature  
722 changes in the source areas of deep-water formation around Antarctica. The similarity of deep-  
723 water temperature estimated by Mg/Ca at ODP Site 1123 in the South Pacific and Antarctic  
724 temperature (Elderfield et al 2012) supports this interpretation, as does the emerging but sparse  
725 evidence for similarity between mean ocean temperature and Antarctic temperature (Haeberli  
726 et al., 2021). [Surface temperatures in the high-latitude Southern Ocean may have been](#)

Deleted: Figs

Deleted: 7

Deleted: 10

Deleted: It

Deleted: the

Deleted: constitute

Deleted: if you will

Deleted: 4

Deleted: This interpretation implies that s

Deleted: were

737 important for regulating deep-ocean heat content, which has implications for deep ocean  
738 circulation and CO<sub>2</sub> storage (Jansen, 2018). Skinner et al. (2007) measured benthic Mg/Ca and  
739 δ<sup>18</sup>O in core MD01-2444 during MIS 3 and concluded that the benthic δ<sup>18</sup>O record cannot be  
740 interpreted as a unique proxy of either deep-water temperature or ice-volume and must contain  
741 a significant local hydrographic component related to the mixing of end member water masses  
742 from the North Atlantic and Southern Ocean which have different δ<sup>18</sup>O values. This is further  
743 supported by similar results from the deep Southern Ocean, where benthic δ<sup>18</sup>O exhibits a  
744 similar (but not identical) pattern to that observed on the Iberian Margin (Gottschalk et al.,  
745 2020), and deep-water temperatures again appear to have decreased during HS4, consistent  
746 with enhanced convection contributing to Antarctic warmth and CO<sub>2</sub> rise (Skinner et al., 2020;  
747 Menviel et al., 2015). In all cases, a global glacioeustatic signal would only be transported  
748 around the globe on a time-scale that is consistent with ocean transport and mixing (i.e.  
749 centuries to millennia) (Primeau and Deleersnijder, 2009), which would oppose any proposal  
750 of benthic δ<sup>18</sup>O tracking global ice volume in synchrony (Gebbie et al., 2012). Indeed, this is  
751 demonstrated by the phasing of benthic δ<sup>18</sup>O, Antarctic temperature, mean ocean temperature,  
752 and sea level on the last deglaciation (Skinner et al., 2005; Baggenstos et al., 2019).

753  
754 As in the latest Pleistocene, stadial events are associated with decreases in benthic δ<sup>13</sup>C for the  
755 past 1.45 Ma, suggesting that surface coolings in the North Atlantic were associated with  
756 perturbations of deep-water ventilation and carbon storage in the deep Atlantic (Martrat et al.,  
757 2007; Shackleton et al., 2000; Skinner et al., 2007). Low δ<sup>13</sup>C values are associated with each  
758 of the glacial terminations when δ<sup>18</sup>O is decreasing and, in some cases, the low δ<sup>13</sup>C values are  
759 prolonged and extend into the early part of the interglacial period (Hodell et al., 2009; Galaasen  
760 et al., 2014, 2020).

Deleted: -sea

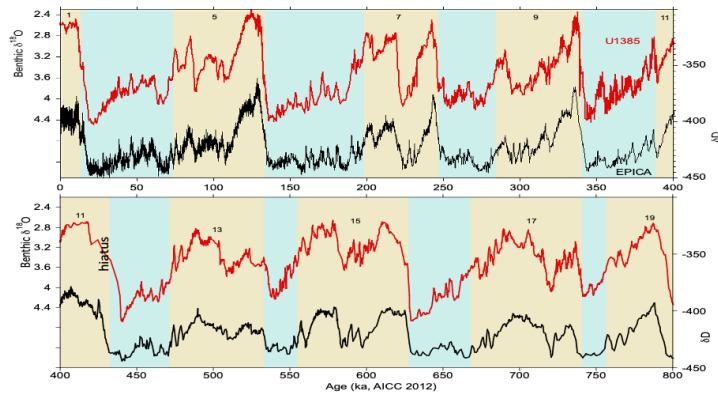


**Figure 13.** Comparison of benthic  $\delta^{18}\text{O}$  from MD01-2444 and Site U1385 on the Iberian Margin and  $\delta\text{D}$  from EPICA Dome C ice core, Antarctica, for the last 800 kyrs.

### 4.3 Phasing of planktic and benthic $\delta^{18}\text{O}$ and the bipolar seesaw

Because of the similarity of the planktic and benthic oxygen isotope records to Greenland and Antarctica, respectively, Shackleton et al. (2000) suggested the relative phasing of inter-hemispheric climate change could be assessed [in depth domain](#) using a single core from the Iberian margin. The lead of [millennial-scale](#) benthic over planktic  $\delta^{18}\text{O}$  in piston cores [from](#) MIS 3 (Shackleton et al., 2000; Skinner et al, 2007) [is observed throughout the](#) Site U1385 [record](#) (Figure 14). This apparent lead of the benthic over the planktic  $\delta^{18}\text{O}$  is more likely the consequence of the different shapes of the benthic (rectangular) and planktic (triangular) signals (Hinnov et al., 2002). Rather than a direct lead/lag relationship between the polar regions, the thermodynamic bipolar seesaw model predicts an anti-correlation between Greenland temperature and the rate of change of Antarctic temperature with the abrupt warmings in Greenland leading the Antarctic cooling onset by about 200 years (WAIS Divide Ice Core members, 2015). The consistent phase relationships between planktic and benthic  $\delta^{18}\text{O}$  during millennial events suggest the oceanic bipolar see-saw was a robust feature of the interhemispheric climate system despite differences in climate background state. For example, the phasing is the same during glacial inception as it is during deglaciations and intermediate ice volume states [such as MIS 3](#). Millennial variation in AMOC and [the](#) thermal bipolar seesaw represent mechanisms by which MCV can be propagated [from the North Atlantic](#) to the broader climate system.

Deleted: 4

Deleted: [

Deleted: ]

Deleted: To evaluate the phasing of MCV, oxygen isotope records of Site U1385 were first high-pass filtered to remove orbital-scale variability. Cross correlation analysis was then performed using the Matlab function xcorr. The filtered planktic and benthic  $\delta^{18}\text{O}$  records are weakly correlated and show an average lead of  $\sim 0.8$  ka for millennial variations in benthic  $\delta^{18}\text{O}$  over those of planktic  $\delta^{18}\text{O}$  for the past 1500 ka (Fig 15A).

Deleted: for the complete record is the same as that observed over shorter time intervals

Deleted: during

Deleted: and for

Deleted: during MIS 38 and 40 (Birner et al., 2016). A cross correlation analysis of the isotope records in the depth domain yields a similar result.

Deleted: time

Deleted: This is equivalent to an antiphase relationship between planktic  $\delta^{18}\text{O}$  (Greenland temperature) and the time derivative of the benthic  $\delta^{18}\text{O}$  signal (Antarctic temperature) from the Iberian margin (Stocker and Johnsen, 2003; Barker et al., 2011). Because taking the derivative of a variable signal can result in noise, the filtered benthic  $\delta^{18}\text{O}$  was first smoothed with a 5-point running mean. Although the correlation is poor, the phase shift is as predicted from the thermal bipolar seesaw model (Fig. 15B).

Deleted: for the past 1.45 Ma

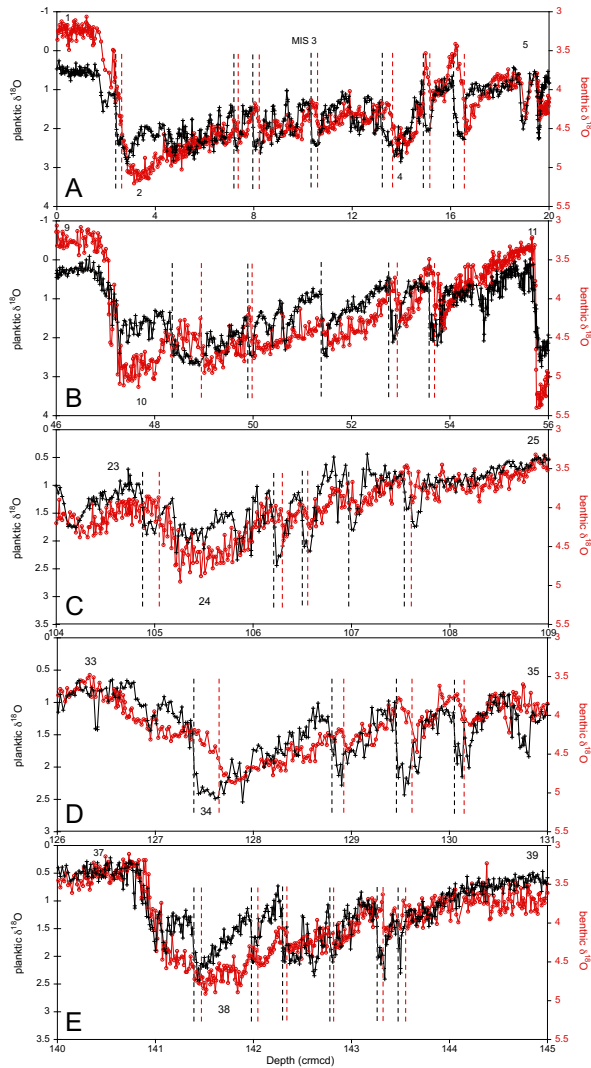
Deleted: . This phasing is similar

Deleted: ;

Deleted: f

Deleted: the

822



823

824

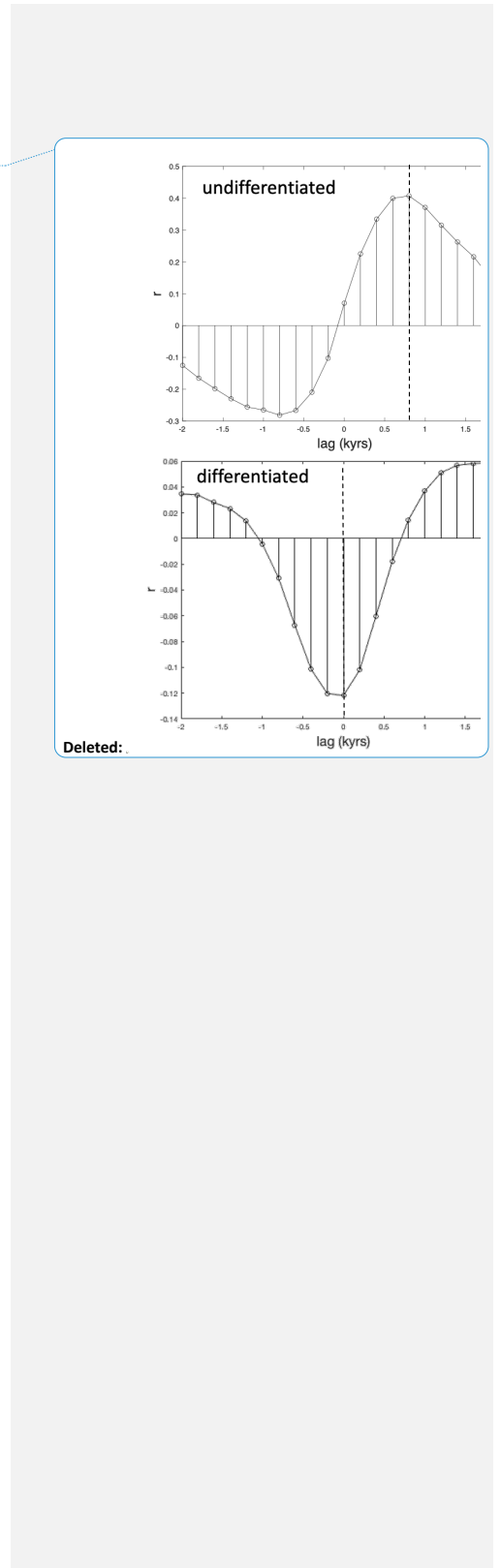
825

826

827

828

**Figure 14.** Examples of the phasing of millennial benthic and planktic  $\delta^{18}\text{O}$  variability in depth domain: (A) MIS 1-5; (B) MIS 9-11; (C) MIS 23-25; (D) MIS 33-35; and (E) MIS 37-39. The vertical dashed lines mark the rapid warmings (decreases) in the planktic  $\delta^{18}\text{O}$  record (black) and decreases in benthic  $\delta^{18}\text{O}$  (red). The decrease in benthic  $\delta^{18}\text{O}$  occurs prior to the decrease in planktic  $\delta^{18}\text{O}$ , which is similar to the phasing observed during MIS 3 (A and Figure 2).

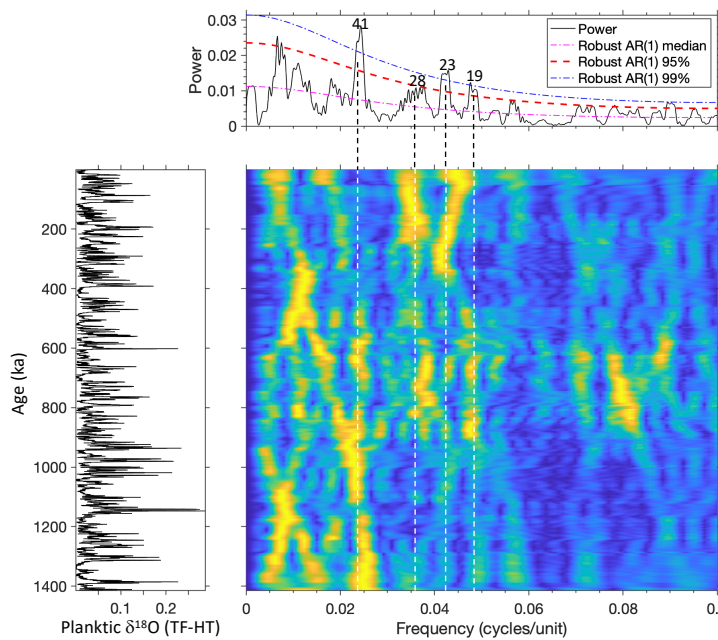


Deleted:

830  
831  
832  
833

#### 4.4 Orbital modulation of MCV

834 To test for amplitude modulation of millennial variability by orbital cycles, we follow the  
835 approach of Hinnov et al. (2002) who analyzed the MD95-2042 record for the last 100 kyr.  
836 We examine the power spectrum of the planktic  $\delta^{18}\text{O}$  and Zr/Sr records after applying a Taner  
837 filter and Hilbert transform. Bandpass filtering was performed on evenly resampled (0.2 kyr)  
838 time series using a Taner filter centered on  $0.55 \pm 0.45$  with a roll-off rate =  $1 \times 10^{12}$ , which has  
839 better leakage suppression outside the stopband compared to the Butterworth filter. The  
840 instantaneous amplitude of the modulating signal was calculated by Hilbert transformation.  
841 The presence of significant orbital frequencies in the power spectrum of the Hilbert transform  
842 indicates orbital modulation of the amplitude of MCV, and the evolutive spectra show how the  
843 orbital modulation of MCV has changed through time (Figs. 15 and 16).



844  
845  
846

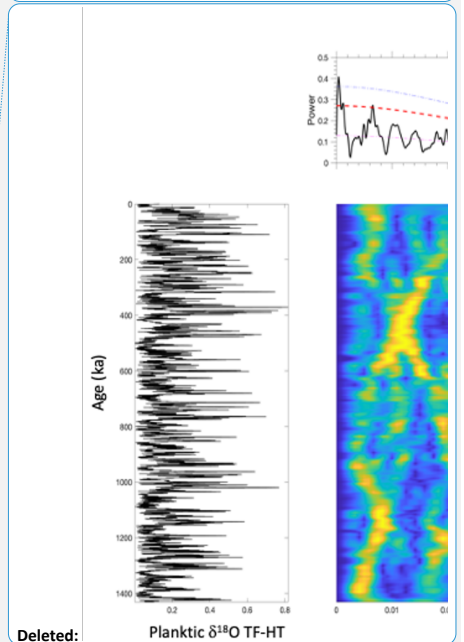
**Figure 15.** Evolutive power spectrum of the amplitude modulation of planktic  $\delta^{18}\text{O}$  as estimated from a Taner filter (TF) centered at  $0.55 \pm 0.45$  and Hilbert transformation (HT) of

**Deleted:** Figure 15. (A) Cross correlation coefficient ( $r$ ) of the filtered signals of planktic and benthic  $\delta^{18}\text{O}$ . Positive offsets denote a lead of benthic  $\delta^{18}\text{O}$  over planktic  $\delta^{18}\text{O}$  by 800 yrs. (B) Cross correlation of planktic  $\delta^{18}\text{O}$  and the time derivative of smoothed and benthic  $\delta^{18}\text{O}$ . Selected examples of the phasing of millennial benthic and planktic  $\delta^{18}\text{O}$  variability in depth domain: (C) MIS 9-11; (D) MIS 23-25; (E) MIS 33-35; and (F) MIS 37-39. The vertical dashed lines mark the rapid warmings (decreases) in the planktic  $\delta^{18}\text{O}$  record and the red arrows indicate decreases in benthic  $\delta^{18}\text{O}$ . In most cases, the decrease in benthic  $\delta^{18}\text{O}$  occurs prior to the decrease in planktic  $\delta^{18}\text{O}$ , which is similar to the phasing observed during MIS 3 (Figure 2).

Deleted: 6

Deleted: 7

Deleted:



Deleted:

Deleted: 6



865 the time series. Sliding window of ~300 kyrs with time domain zero padding and a step equal  
866 to the sampling rate of the time series (~0.2 kyrs).

867

868 The power spectra of planktic  $\delta^{18}\text{O}$  and Zr/Sr are similar and support orbital modulation of the  
869 amplitude of the millennial band by Earth's orbital parameters (e.g., 19, 23, 28, 41 kyrs). The  
870 41-kyr obliquity dominates the modulation of MCV between 1450 and ~900 ka with a weak  
871 precession component (Figs. 15 and 16). At ~900 ka, power develops at ~28 kyrs and  
872 precession strengthens, especially in the Zr/Sr record (Fig. 16). The 28 kyr cycle is not entirely  
873 unexpected because it has been widely reported in late Pleistocene ice core and marine  $\delta^{18}\text{O}$   
874 records (Huybers and Wunsch, 2004; Lisiecki and Raymo, 2005; Lourens et al. 2010). We note  
875 that the theoretical obliquity signal contains a secondary peak at ~29 ky as well as 54 ky (Laskar  
876 et al., 2004), but their spectral power seem too weak to be of any direct climatic significance.  
877 Instead, the 28-kyr cycle has been interpreted by Lourens et al. (2010) as resulting from the  
878 sum frequencies between the 41-kyr cycle and its multiples of 82-kyr (i.e.  $1/82 + 1/41 = 1/27.3$ )  
879 and 123-kyr (i.e.  $1/123 + 1/41 = 1/30.8$ ). However, the 28-kyr power could also result from the  
880 difference of frequencies between multiples of the 41-kyr cycle and the main precession  
881 components (e.g.,  $1/21 - 1/82 = 1/28.2$ ). Liebrand and de Bakker (2019) applied bispectral  
882 analysis techniques to the LR04 benthic  $\delta^{18}\text{O}$  signal and showed that a large part of the  
883 precession (spectral) energy could have been transferred to the lower frequencies of obliquity  
884 and its multiples in the course of the Quaternary, and especially during the MPT. In this respect,  
885 the presence of a strong precession signal in both the planktonic  $\delta^{18}\text{O}$  and Zr/Sr records of  
886 U1385 could be partially responsible for the occurrence of the ~28-kyr beat, but additional  
887 bispectral analyses is required to further unravel these energy transfers. At ~650 ka, the 41-kyr  
888 and 28-kyr power of obliquity declines substantially and the spectrum is marked by lower-  
889 frequency power (80-120 kyrs), which is difficult to interpret in the evolutive spectrum because  
890 of the relatively short window size (~300 kyrs). This may reflect an increase in eccentricity  
891 modulation of MCV or modulation by multiples of the obliquity and precession cycles, or a  
892 change in the non-linear energy transfer between orbital components across the MPT (Liebrand  
893 and de Bakker, 2019).

Deleted: e

Deleted: 16

Deleted: 7

Deleted: 7

Deleted: The 28-kyr cycle is a common feature of Pleistocene foraminiferal  $\delta^{18}\text{O}$  records (Huybers and Wunsch, 2004; Lisiecki and Raymo, 2005; Lourens et al., 2010). The 28-kyr cycle has been interpreted as resulting from non-linear interactions (combination tones) between eccentricity (quasi-100 kyrs) and precession (23 kyr) or obliquity (41 kyr). Lourens et al. (2010) suggested the 28-kyr cycle reflects the sum frequency of the primary 41-kyr cycle and its multiples (82 and 123 ky), and results from a non-linear response of the glacial cycles to obliquity forcing.

Formatted: Font: Symbol

Formatted: Superscript

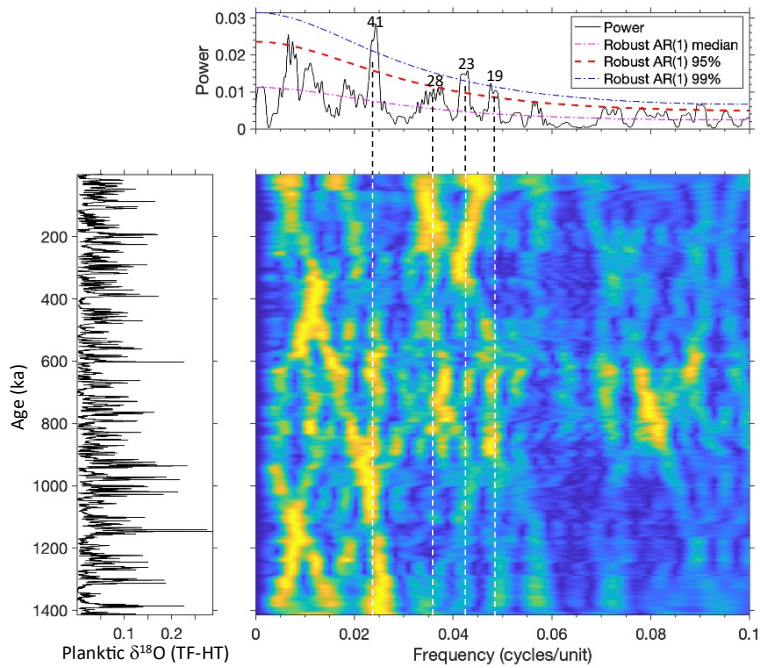
Formatted: Font: Symbol

Formatted: Superscript

Deleted: .



909

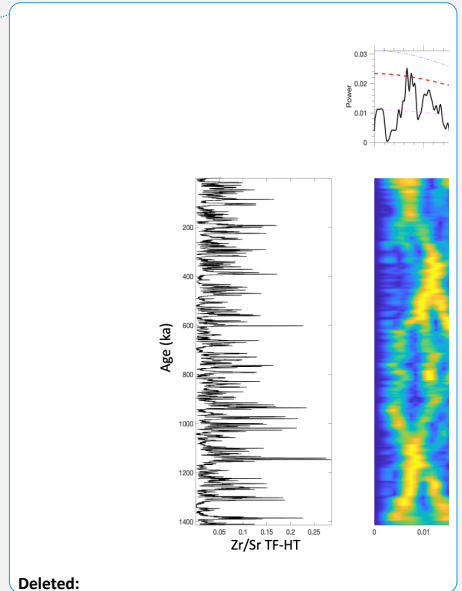


910

911 **Figure 16.** Same as Figure 15, but for Zr/Sr.

912

913 The early Pleistocene interval from 1200-1440 ka provides strong evidence for a relationship  
 914 between the occurrence of MCV and obliquity (Fig. 12). MCV increases during times of low  
 915 obliquity, displaying a threshold response such that it increases each time the obliquity drops  
 916 below  $\sim 23.5^\circ$ . [The relationship between MCV and obliquity is not a result of orbital tuning as](#)  
 917 [the chronology was derived by tuning the color \( \$L^\*\$ \) to precession and is independent of](#)  
 918 [obliquity \(Hodell et al., 2015\).](#) It is uncertain, however, if the increased millennial variability  
 919 is the direct (i.e., fast-acting) result of [obliquity through its effect on the mean insolation](#)  
 920 [\(Berger et al., 2010\) and mainly on the total summer insolation at high latitudes \(e.g., lowered](#)  
 921 [insolation, colder temperature, sea ice expansion\) or on the meridional insolation gradient.](#)  
 922 [Alternatiely,](#) low obliquity secondarily leads to increased ice volume, [raised](#) ice-sheet height  
 923 and lowered sea level (see Discussion section 4.5) -- all of which have been proposed as a  
 924 threshold for MCV (McManus et al., 1999; Zhang et al., 2014).



Deleted:

Deleted: 7

Deleted: 6

Deleted: 3

Deleted: reduced insolation at high latitude caused by low obliquity ...

Deleted: whether

932  
933 Some modelling experiments have demonstrated increased MCV during times of low obliquity  
934 in the absence of freshwater forcing (Friedrich et al., 2010; Brown and Galbraith, 2016;  
935 Galbraith and de Lavergne, 2018). The obliquity threshold observed for the early Pleistocene  
936 is highly suggestive of a non-linear system that is influenced by orbital cycles. For example,  
937 sea ice expansion during times of low obliquity may provide strong albedo-feedback  
938 amplification, resulting in a non-linear response (Tuenter et al., 2005). As the mean position of  
939 the sea ice edge expands to lower latitudes, the region of deep water formation moves from the  
940 Norwegian-Greenland Sea to south of Iceland, shifting the AMOC with respect to the mean  
941 atmospheric precipitation field where precipitation exceeds evaporation, thereby making the  
942 system less stable (Sevellec and Fedorov, 2015, Friedrich et al., 2010).

943  
944 The relationship between low obliquity and enhanced MCV persists after 1.2 Ma and is  
945 expressed as increased millennial variability associated with the transitions from [interglacial](#)  
946 [to glacial stages, which is always associated with declining obliquity](#) (Tzedakis et al., 2012).  
947 In view of this, Tzedakis et al. (2012) proposed the end of interglacials could be defined as  
948 three thousand years (kyr) before the reactivation of MCV at the time of glacial inception. Low  
949 obliquity is important for controlling ice accumulation at the start of a glaciation because ice  
950 growth begins at high latitudes (and altitudes) where the effect of obliquity on summer  
951 insolation is strongest (Vettoretti and Peltier, 2004). Lower obliquity decreases the summer  
952 insolation at high latitudes, reduces seasonality and strengthens the insolation gradient between  
953 low and high latitudes, thereby increasing the meridional heat and moisture flux to the high  
954 latitudes (Mantis, 2011). The increased heat transport does not balance the direct cooling  
955 effects of obliquity through reduced insolation at high latitude. Increased moisture transport  
956 towards the poles provides the fuel needed for growing ice-sheets (Vimeux et al. 1999; Raymo  
957 and Nisancioglu 2003). The combination of reduced temperature and increased moisture flux  
958 are the two ingredients needed for rapid ice sheet growth during glacial inceptions. Precession  
959 and atmospheric CO<sub>2</sub> play secondary roles at glacial inceptions that may reinforce or delay  
960 increased ice accumulation depending on CO<sub>2</sub> concentration and the phasing of precession and  
961 obliquity (Vettoretti and Peltier, 2004).

962  
963 Modelling studies suggest that orbital forcing may play a more direct role in the onset of MCV  
964 at the end of interglacial periods. Using LOVECLIM1.3, Yin et al. (2021) found a threshold  
965 response to decreasing summer insolation related to both precession and obliquity. When  
966 summer insolation falls below a critical value, a strong, abrupt weakening of AMOC is

Deleted: inter

968 triggered as sea ice expands in the Nordic and Labrador Seas. The transition into a cooler mean  
969 climate state is accompanied by high-amplitude temperature variations lasting for several  
970 thousand years (Yin et al., 2021).

971  
972 Zhang et al. (2021) used a fully coupled climate model and found that changes in Earth's orbital  
973 geometry can directly affect MCV during intermediate glacial states (e.g., MIS 3). Both  
974 obliquity and precession play a role in AMOC stability (Zhang et al., 2021; Yin et al., 2021)  
975 through its effect on mean insolation at high latitudes and eccentricity-modulated precession  
976 through its low-latitude effect on the subtropical hydrologic budget and salinity of the North  
977 Atlantic basin.

Deleted: -- obliquity

978  
979 MCV can also result from orbital forcing that is expressed as subharmonics and combination  
980 tones of the primary orbital cycles. Using bispectral analysis, Hagelberg et al. (1994)  
981 demonstrated that approximately a third of the variability in the frequency band ranging from  
982 1/15 to 1/2 kyr originates from the transfer of spectral energy from the lower-frequency  
983 Milankovitch band (see also Liebrand and de Bakker, 2019). A case in point is the 11- and 5.5-  
984 kyr cycles found in MIS 21 and 19, respectively, that have been attributed to the second and  
985 fourth harmonics of the primary precession cycles (Ferretti et al., 2015; Sanchez-Goni et al.,  
986 2016). Berger et al. (2006) suggested the double maximum that occurs in daily irradiation at  
987 tropical latitudes includes a suborbital insolation forcing at 11-kyr and 5.5-kyr periods related  
988 to precession harmonics.

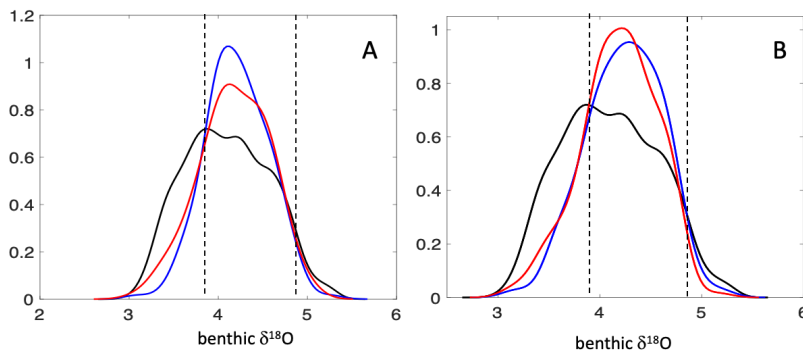
Deleted: Zhang et al. (2021) proposed a physical mechanism for MCV related to the effect of eccentricity-modulated precession through its low-latitude effect on the subtropical hydrologic budget and salinity of the North Atlantic basin.

#### 991 **4.5 State dependence of MCV**

992  
993 Orbital changes may influence MCV directly through fast processes (e.g., sea ice) or more  
994 indirectly through slow changes in ice sheet configuration (volume or height) and sea level. On  
995 the basis of a 500-ka-long record of ice-rafted detritus and summer SST from Site 980 at 55 °N  
996 in the Rockall Trough, McManus et al. (1999) suggested that MCV was enhanced during times  
997 of intermediate ice volume as defined by a window or "sweet spot" when MCV was most active  
998 during times of intermediate glacial states (Sima et al., 2004; Galbraith and de Lavergne, 2018).  
999 MCV is suppressed under full interglacial conditions and during some peak glaciations. The  
1000 concept of increased MCV during times of intermediate ice volume is supported by  
1001 observations from the last glacial cycle when MCV was relatively suppressed during MIS 2  
1002 and 4 and strong during MIS 3. MCV was also frequent during glacial periods of the early  
1003 Pleistocene between 1.45 and 1.25 Ma when glacial benthic  $\delta^{18}\text{O}$  values fell entirely within the

1009 millennial window (Fig. 5). After 1.25 Ma, the benthic  $\delta^{18}\text{O}$  threshold is crossed slowly during  
1010 glacial inception and more quickly at glacial terminations (Sima et al., 2004) with some, but  
1011 not all, full glacial periods marked by reduced MCV.

1012  
1013 We tested whether there is a statistically significant tendency for millennial events to occur  
1014 within a certain range of benthic  $\delta^{18}\text{O}$  values at Site U1385. The FindPeak algorithm in MatLab  
1015 returns the age of each event identified, which is then used to lookup its corresponding benthic  
1016  $\delta^{18}\text{O}$  value. The  $\delta^{18}\text{O}$  values are concatenated to form a subpopulation of benthic  $\delta^{18}\text{O}$  values  
1017 corresponding to millennial events that is compared with the full population of benthic  $\delta^{18}\text{O}$   
1018 values (Fig. 17A&B). A two-sample Kolmogorov-Smirnov (K-S) test is used to evaluate if the  
1019 two populations are from the same or different continuous distributions and whether the tail of  
1020 the millennial subpopulation distribution is smaller than the full population of benthic  $\delta^{18}\text{O}$   
1021 values.



1022  
1023 **Figure 17.** Probability density estimate of benthic  $\delta^{18}\text{O}$  for all values (black), interstadial (red);  
1024 and stadial (blue) events for planktic  $\delta^{18}\text{O}$  (A) and Zr/Sr (B). Vertical dashed lines represent  
1025 benthic  $\delta^{18}\text{O}$  threshold values for MCV that define the millennial window.

1026  
1027 For millennial events identified in both planktic  $\delta^{18}\text{O}$  and Zr/Sr, the millennial benthic  $\delta^{18}\text{O}$   
1028 population was significantly different from the full population at 95% confidence, and the tail  
1029 of the millennial populations was significantly smaller than that of the full  $\delta^{18}\text{O}$  population.  
1030 Millennial events are clearly less frequent at the low (warm) end of the benthic  $\delta^{18}\text{O}$   
1031 distribution suggesting reduced MCV during full interglacial periods. We estimate the lower  
1032 benthic  $\delta^{18}\text{O}$  threshold to be  $\sim 3.8\text{‰}$  for both planktic  $\delta^{18}\text{O}$  and Zr/Sr (note that  $0.64\text{‰}$  must  
1033 be subtracted from this value to convert to the *Cibicidoides* scale) (Fig. 10C&D). The  $\delta^{18}\text{O}$

Deleted: 8

Deleted: 8

Deleted: 1

1037 threshold for MCV may differ depending on the record and proxy used to identify millennial  
1038 variability (IRD, SST, planktic  $\delta^{18}\text{O}$ , etc.) and may be non-stationary through time. For  
1039 example, Bailey et al. (2010) suggested that the  $\delta^{18}\text{O}$  threshold for the late Pliocene (MIS G4  
1040 at ~2640 ka and MIS 100 at ~2520 ka) was 0.45‰ lower than that of the late Pleistocene. For  
1041 the period 1240 to 1320 ka at Site U1385, Birner et al. (2016) suggested the threshold was  
1042 3.2‰ on the *Cibicidoides* scale which is equivalent to 3.84‰ on the *Uvigerina* scale. This is  
1043 the same value we have estimated for the entire 1.5 million yr interval, suggesting the benthic  
1044  $\delta^{18}\text{O}$  threshold has not changed significantly at Site U1385. The existence of an upper  $\delta^{18}\text{O}$   
1045 threshold above which millennial variability is suppressed during peak glacial conditions is less  
1046 clear from the probability density estimates (Fig. 17). However, several of the late Pleistocene  
1047 glacial intervals (MIS 2, 4, 6, 10, 12, 16) show a pattern of strong MCV associated with glacial  
1048 inception that decreases towards full glacial conditions (>4.8‰ on the *Uvigerina* scale),  
1049 suggesting reduced MCV during maximal glacial conditions.

1050  
1051 The physical significance of the benthic  $\delta^{18}\text{O}$  thresholds that define the millennial window is  
1052 uncertain. Although several studies have suggested that MCV is related to ice volume, it's not  
1053 certain which part of the climate-cryosphere system was responsible. Several processes have  
1054 been suggested to trigger increased MCV including sea level dropping below a critical sill  
1055 depth (e.g., Bering Sea; De Boer and Nof, 2004), the effect of ice sheet height on winds (Zhang  
1056 et al., 2014), iceberg calving and freshwater fluxes to the oceans, or direct orbital forcing  
1057 (Friedrich et al., 2010; Zhang et al., 2021; Yin et al., 2021).

1058  
1059 McManus et al. (1999) suggested that MCV was enhanced with a sea level lowering of as little  
1060 as 30 m below modern. This may correspond to a critical sill depth such as the Bering Sea,  
1061 which has a sill depth of ~45 m. De Boer and Nof (2004) proposed that the onset and cessation  
1062 of flow through the Bering Strait was responsible for the switch between stable and unstable  
1063 states of glacial versus interglacial climate. A restricted Bering Strait increases the sensitivity  
1064 of AMOC to freshwater perturbation by blocking the escape route of freshwater to the Pacific  
1065 via the Arctic (Poppelmeier et al., 2020; Hu et al., 2012a,b). Freshwater can accumulate in the  
1066 North Atlantic more readily with a closed Bering Strait, thereby increasing surface  
1067 stratification and leading to AMOC instability.

1068  
1069 Because benthic  $\delta^{18}\text{O}$  also depends on bottom temperature, the threshold could also be related  
1070 to surface temperature conditions in the source area of deep-water formation. For example, the

Deleted: 8

1072 benthic  $\delta^{18}\text{O}$  threshold could correspond to crossing the freezing point of seawater in deep-  
1073 water source areas in the North Atlantic, which would result in increased sea ice formation and  
1074 shift the region of deep-water formation to the south where the AMOC is more susceptible to  
1075 oscillation (Sevellec and Fedorov, 2015).

1076  
1077 Galbraith and de Lavergne (2018) suggested that D-O-like variability in AMOC was more  
1078 likely to occur under a ‘sweet spot’ of interrelated conditions that included low obliquity, low  
1079  $\text{CO}_2$  and a low-elevation Laurentide ice sheet. By analyzing dust flux from the Dome Fuji ice  
1080 core (Antarctica) over the last 720 kys, Kawamura et al. (2017) also concluded that MCV was  
1081 more likely during times of intermediate glacial states. Because glacial climate state is  
1082 ultimately affected by orbital geometry, an inherent link must exist between climate variability  
1083 on orbital and suborbital time scales (see discussion in section 4.4).

#### 1084 4.6 MCV across the Middle Pleistocene Transition

1085  
1086 The MPT ~~is generally considered to have occurred~~ between  $\sim 1200$  and 650 ka ~~although the~~  
1087 ~~exact timing is dependent upon the proxy signal and method used to define the shift in~~  
1088 ~~frequency (Berends et al., 2021). The benthic  $\delta^{18}\text{O}$  record involved an increase in amplitude~~  
1089 ~~and a shift in~~ the dominant period of glacial-interglacial cycles ~~from 41 kyrs before  $\sim 1200$  ka~~  
1090 ~~to quasi-100 kyrs after 650 ka (Clark et al., 2006). Some studies have suggested that MCV was~~  
1091 ~~less frequent during the early Pleistocene and increased across the MPT as the size of Northern~~  
1092 ~~Hemisphere ice sheets expanded (Larrasoana et al., 2003; Weirauch et al., 2008; Bolton et al.,~~  
1093 ~~2010). Others have found evidence for equally strong millennial variability in the early~~  
1094 ~~Pleistocene as the late Pleistocene (Raymo et al., 1998; McIntyre et al., 2001; Tzedakis et al.,~~  
1095 ~~2015; Grütznér and Higgins, 2010; Hodell et al., 2008; Birner et al., 2016). Still others have~~  
1096 ~~suggested MCV (as represented by IRD events) was more frequent but less intense prior to 650~~  
1097 ~~ka because the climate system spent more time in the millennial window during the early~~  
1098 ~~Pleistocene (Hodell et al., 2008; Hodell and Channell, 2016) and rarely exceeded the upper~~  
1099 ~~benthic  $\delta^{18}\text{O}$  threshold before 650 ka.~~

1100  
1101  
1102 The planktic  $\delta^{18}\text{O}$  and Zr/Sr records of Site U1385 clearly demonstrate that MCV was strong  
1103 during glacial stages both before and after the MPT. The main difference across the MPT is  
1104 that whereas MCV persists throughout the glacial periods prior to 1200 ka, it is most prevalent  
1105 on the transitions both into and out of glacial states (i.e., inceptions and terminations) and  
1106 during times of sustained intermediate ice volume, such as MIS 3. Beginning at 650 ka (MIS

- Deleted: occurred
- Deleted: an
- Deleted: d
- Deleted: global ice volume
- Formatted: Font: Symbol
- Formatted: Superscript
- Deleted: as
- Deleted: shifted
- Deleted: (Clark et al., 2006)

1114 16) following the MPT, MCV is suppressed during some of the strongest glacial periods  
1115 associated with the growth of oversized continental ice sheets, which Raymo (1997) refers to  
1116 as "excess ice".

1117  
1118 A change occurred in the orbital modulation of MCV across the MPT as expressed in changes  
1119 in the evolutive spectra of the Taner filter-Hilbert transform of the Zr/Sr and planktic  $\delta^{18}\text{O}$   
1120 (Figs. 15 and 16). Prior to ~900 ka, the amplitude modulation of MCV was dominated by 41-  
1121 kyr obliquity. Obliquity continues to modulate the amplitude of MCV from 900 to 600 ka, but  
1122 with an increase in precession and the addition of a possible combination tone (28 kyrs) of the  
1123 41-kyr cycle.

1124  
1125 By ~600 ka, the power of obliquity declines and the spectra become more complex with greater  
1126 modulation at lower frequencies (e.g, 100±20 kyrs). Hodell et al. (2008) noted a similar change  
1127 in the amplitude modulation of the Si/Sr IRD proxy at Site U1308 in the central North Atlantic  
1128 IRD belt when, at ~650 ka, the power of the 41-kyr obliquity cycle decreased and quasi-100-  
1129 kyr power increased. Hodell and Channell (2016) also observed that millennial variability in  
1130 the Si/Sr IRD proxy was proportional to the power in the precessional band, suggesting an  
1131 amplitude modulation of MCV by precession. Precession plays a greater role in modulating  
1132 the amplitude of MCV in the late Pleistocene, in agreement with its steady increase in  
1133 importance throughout the Quaternary (Liautaud et al., 2020).

1134  
1135 At 0.65 Ma, the development of massive ice sheets on North America (Batchelor et al., 2019)  
1136 introduced a new type of MCV related to dynamic instability of the Laurentide Ice Sheet in the  
1137 region of Hudson Strait, which was expressed by the occurrence of Heinrich layers in North  
1138 Atlantic sediment beginning in MIS 16 (Hodell et al., 2008; Hodell and Channell, 2016).  
1139 Heinrich events tend to occur late in the glacial cycle and are associated with glaciations of  
1140 long duration (Hodell et al., 2008). They are distinct from background IRD events in their  
1141 magnitude, frequency and duration, and their impact on the global climate system was more  
1142 widespread (Marshall and Koutnik, 2006). MCV associated with late Pleistocene terminations  
1143 after 0.65 Ma are closely related to freshwater fluxes from the decay of oversized ice sheets,  
1144 which play an important role in the progression of glacial terminations (Wolff et al., 2009;  
1145 Barker and Lohman, 2021).

1146  
1147 **4.7 Influence of MCV on glacial-interglacial cycles**  
1148

Deleted: 0

Deleted: 1

Deleted: At the end of the MPT (

Deleted: )

1153 Ice dynamics may be an effective mechanism for propagating high-frequency variability to  
1154 longer, orbital timescales (Verbitsky et al., 2019). For example, Siddall et al. (2006) suggested  
1155 that sustained ice-sheet growth through a glacial cycle requires the absence of MCV. Niu et al.  
1156 (2019) proposed that the presence of strong MCV may prevent an ice sheet from reaching its  
1157 maximum size owing to surface mass balance effects. If true, then sustained MCV throughout  
1158 the glacial periods of the early Pleistocene may have prevented ice sheets from growing as  
1159 large as their late Pleistocene counterparts. In contrast, strong MCV on glacial inceptions may  
1160 have significantly slowed ice sheet development giving rise to the sawtooth shape of the late  
1161 Pleistocene benthic  $\delta^{18}\text{O}$  signal. Ice sheets could only reach their maximum size during the  
1162 latter part of the glacial cycle once MCV was suppressed.

1163  
1164 The exact cause-effect relationship between MCV and ice sheet size is difficult to ascertain.  
1165 Did ice sheets grow larger in the late Pleistocene because MCV was suppressed or did large  
1166 ice sheets lead to a suppression of MCV during full glacial conditions? In either case, orbital  
1167 and millennial-scale variability cannot be considered separately from one another because they  
1168 interact. Verbitsky et al. (2019) demonstrated that ice sheet non-linearity allows MCV to  
1169 propagate upscale and influence ice-age dynamics. In addition, non-linear ice-flow dynamics  
1170 can propagate downscale and affect the millennial part of the spectrum.

1171  
1172 MCV constitutes a source of [high-frequency variability](#) on orbital time scales, which may  
1173 enhance the phase-locking of the response of the climate system to orbital forcing (Hodell and  
1174 Channell, 2016). The theory of stochastic resonance has long been considered as a possible  
1175 mechanism to explain how the climate system can be synchronized with relatively weak orbital  
1176 forcing (Benzi et al., 1982). The "noise" for stochastic resonance is often assumed to be random  
1177 and white. ~~Although MCV is not noise, it~~ provides a source of [high-frequency variability](#) in  
1178 the climate system whose amplitude varies with climate background state -- i.e., relatively  
1179 "[active](#)" during glacials and "[quiet](#)" during interglacials. Such oscillations in amplitude may be  
1180 relevant for stochastic or coherence resonance in which the signal–noise resonance is important  
1181 for phase locking (Liu and Chao, 1998). For example, glacial-interglacial variations during the  
1182 early Pleistocene may consist of a resonant system in which the intensity of millennial  
1183 variability is responding to obliquity-controlled changes in climate background state and, in  
1184 turn, changes in the amplitude of MCV may aid in phase locking the climate system to the  
1185 obliquity period. [Stochastic forcing by millennial and centennial climate variability may have](#)

Deleted: High-frequency

Deleted: noise

Deleted: ,

Deleted: but

Deleted: noise

Deleted: to

Deleted: noisy

Deleted: noise



1194 [also been a crucial factor for the frequency-band change associated with the MPT \(Mukhin et](#)  
1195 [al., 2019\).](#)

Formatted: Font: Times, (Asian) Chinese (China)

1196  
1197

#### 1198 **4.8 MCV and atmospheric CO<sub>2</sub> variations**

1199

1200 Because nearly all the rapidly exchangeable carbon in the ocean-atmosphere system is  
1201 contained in the deep ocean, atmospheric greenhouse gas variations in ice cores are intimately  
1202 linked to carbon storage in the deep ocean. Variations in benthic carbon isotopes at Site U1385  
1203 demonstrate that the millennial changes in planktic  $\delta^{18}\text{O}$  are not only a feature of surface  
1204 climate on the Iberian margin, but are crucially linked with changes in deep-water ventilation.  
1205 Decreases in benthic  $\delta^{13}\text{C}$  are associated with increases in planktic  $\delta^{18}\text{O}$ , indicating reduced  
1206 ventilation of the deep North Atlantic during cold stadial events. A relationship between  
1207 atmospheric CO<sub>2</sub> and centennial-millennial events in the North Atlantic exists for the last  
1208 glaciation and deglaciation (Marcott et al., 2014; Bauska et al., 2021) as well as for older  
1209 periods such as MIS 6 (Shin et al., 2020) and the MIS 11-10 transition (Nehrbass-Ahles et al.,  
1210 2020).

1211

1212 We suggest MCV may be involved in setting the minimum CO<sub>2</sub> values attained during glacial  
1213 periods. Millennial variability in AMOC provides a mechanism by which deep-sea CO<sub>2</sub> can be  
1214 degassed to the atmosphere. When MCV was strong during MIS 3, CO<sub>2</sub> varied between 200  
1215 and 220 ppm and the lowest sustained CO<sub>2</sub> levels of 180-190 ppm were only achieved during  
1216 MIS 2 when MCV was suppressed during peak glacial conditions. By analogy with MIS 3, the  
1217 persistently strong MCV that occurred throughout the glaciations of the early Pleistocene  
1218 (1.45-1.25 Ma) may have prevented CO<sub>2</sub> from reaching values as low as those attained during  
1219 the late Pleistocene because CO<sub>2</sub> was episodically released from the deep-sea reservoir during  
1220 strong millennial-scale AMOC events. In the early Pleistocene, boron isotope reconstructions  
1221 suggest that fluctuations in CO<sub>2</sub> varied in phase with obliquity and benthic  $\delta^{18}\text{O}$  (Chalk et al.,  
1222 2017; Dyez et al. 2018). The threshold-type behaviour of MCV during the 41-kyr cycles of the  
1223 early Pleistocene may have served as an important mechanism for linking internal climate  
1224 dynamics with external astronomical forcing by regulating carbon storage in the deep-sea.

1225

1226 Evidence from Site U1385 for an active oceanic thermal bipolar see-saw during most of the  
1227 prominent stadials during glacials of the 41-kyr world (Birner et al. 2016) supports a similar  
1228 mechanism of CO<sub>2</sub> degassing via the Southern Ocean as that in MIS 3. Although CO<sub>2</sub> records  
1229 are fragmentary before 800 ka, there is evidence for elevated glacial CO<sub>2</sub> with minimum values

1230 of 220 ppm during glacial periods between 1 and 1.25 Ma during the early MPT (Yan et al.,  
1231 2019; Higgins et al. 2015; Chalk et al., 2017; Hönisch et al, 2012), and glacial CO<sub>2</sub> values may  
1232 have been higher still before 1.25 Ma (Yan et al., 2019; Martinez-Botí et al., 2015).

1233  
1234 We have emphasized the role that MCV may play in setting atmospheric CO<sub>2</sub> concentrations  
1235 but others have suggested that, in contrast, atmospheric CO<sub>2</sub> may have a controlling influence  
1236 on millennial-scale climate oscillations (Zhang et al., 2017; Vettoretti et al., 2022). Using an  
1237 Earth system model, Vettoretti et al. (2022) demonstrated that nonlinear self-sustained climate  
1238 oscillations appear spontaneously within an intermediate window of glacial-level atmospheric  
1239 CO<sub>2</sub> concentrations between ~190 and 225 ppm.

1240  
1241 **Conclusion**  
1242

1243 The recognition of MCV in Greenland ice cores in the early 1980s ushered in the study of  
1244 paleoceanographic records at a resolution that is at least 10 times greater than previous orbital-  
1245 scale studies. Although the initial focus was on the last deglaciation and MIS 3, several long  
1246 records of MCV are beginning to emerge (Hodell et al., 2008; Hodell and Channell, 2016;  
1247 Hodell et al., 2015; Barker et al., 2021, 2022), thereby providing an opportunity to document  
1248 the long-term relationships of climate variability on orbital and millennial timescales and their  
1249 interactions. Consistent with previous findings, the U1385 record demonstrates that MCV was  
1250 a persistent feature of intermediate glacial climate states for the last 1.45 Ma, including the 41-  
1251 kyr world of the early Pleistocene prior to the MPT.

1252  
1253 During glacial periods from 1.45 to 1.25 Ma, the amplitude of MCV was strongly modulated  
1254 by changes in Earth's obliquity and exhibited threshold behaviour typical of a non-linear  
1255 system. Beginning at 1.2 Ma at the start of the MPT, MCV becomes more focused on glacial  
1256 inceptions, terminations and periods of intermediate ice volume. One of the recurrent patterns  
1257 is that strong MCV almost always occurs at glacial inception and continues through the period  
1258 of ice growth under conditions of declining insolation forced mainly by obliquity and  
1259 secondarily by precession and CO<sub>2</sub>. During the MPT (1.2-0.65 Ma), obliquity continues to  
1260 influence MCV but in a non-linear fashion evidenced by the appearance of combination tones  
1261 (28 kyrs) of the 41-kyr cycle (Figs. 15 and 16) in the power spectrum of MCV amplitude  
1262 modulation. Near the end of the MPT at 650 ka, MCV amplitude modulation by obliquity  
1263 wanes as quasi-periodic 100 kyr and precession power increases. Precession plays a greater

Deleted: t

Deleted: 9

Deleted: 10

1267 role in modulating the amplitude of MCV in the late Pleistocene consistent with the steady  
1268 increase in precession power throughout the Quaternary (Liautaud et al., 2020).

1269 Dansgaard-Oeschger events during MIS 3 are the archetypal example of millennial variability  
1270 and considerable effort has been directed towards documenting these events globally, including  
1271 the use of numerical models to understand their cause(s). MIS 3 is exceptional relative to the  
1272 other latest Pleistocene glaciations in terms of the high number of millennial events and there  
1273 appears to be no period like it during the past 1200 ka. The strong, continuous millennial  
1274 variability exhibited during MIS 3 is more similar to the millennial variability observed during  
1275 glacial cycles of the early Pleistocene from 1440 to 1200 ka (Birner et al., 2016). This similarity  
1276 is not entirely unexpected considering that benthic  $\delta^{18}\text{O}$  values were about the same during  
1277 early Pleistocene glacial stages as those during MIS 3, indicating the climate system spent a  
1278 prolonged time in an intermediate glacial state. Our analysis of MCV at Site U1385 supports  
1279 the concept of a millennial window or sweet spot defined by a lower benthic  $\delta^{18}\text{O}$  threshold of  
1280  $\sim 2.9\text{‰}$  below which MCV is suppressed during full interglacial conditions. The upper benthic  
1281  $\delta^{18}\text{O}$  threshold is less robust despite the fact that some glacial cycles in the late Pleistocene  
1282 show a clear pattern of reduced amplitude of MCV as the glacial maximum is approached.  
1283 Although the exact physical significance of the benthic  $\delta^{18}\text{O}$  threshold remains uncertain with  
1284 many candidates (ice volume, ice height, sea level, sea ice, deep-water temperatures, etc.),  
1285 MCV is strongest during intermediate glacial states.

1287  
1288 Climate variability on orbital and suborbital time scales are coupled and interact in both  
1289 directions. An example of downscale interaction is the modulation of the amplitude and/or  
1290 frequency of MCV by Earth's orbital configuration either through the direct effects of  
1291 insolation or more indirectly through ice sheet growth. Some MCV may also be related to  
1292 harmonics or combination tones of the orbital cycle (Hagelberg et al., 1994). MCV can exert  
1293 an upscale influence on orbital times scales through its effect on ice sheet dynamics (Verbitsky  
1294 et al., 2019) or on atmospheric  $\text{CO}_2$  by changing carbon storage in the deep-sea. MCV is also  
1295 a source of noise on glacial-interglacial timescales that may affect the resonance of internal  
1296 climate change with external orbital forcing.

1297  
1298 In addition to documenting MCV, the planktic and benthic isotope records from Site U1385  
1299 provide unprecedented detail of the amplitude and shapes (waveforms) of the glacial cycles on  
1300 orbital time scales for the last 1.45 Ma. We emphasize our record is from a single site and

1301 should be compared with other records from higher latitude in the North Atlantic (e.g., Barker  
1302 et al., 2021, 2022) and elsewhere (Sun et al., 2021) in order to map geographical differences  
1303 over time and develop confidence in the palaeoceanographic interpretations set out here. This  
1304 study is also limited to the last 1.45 Ma and we cannot determine the extent to which MCV  
1305 was present during glacial periods beyond this time. [In late 2022 \(12 Oct-12 Dec\)](#), IODP  
1306 Expedition 397 [returned](#) to the Iberian margin and [extended the record of Site U1385 to 4.5](#)  
1307 [Ma in the early Pliocene \(Hodell et al., 2023\)](#). [The new sediment cores recovered during](#)  
1308 [Expedition 397 \(Iberian Margin Paleoclimate\) will document](#) how orbital and millennial  
1309 variability co-evolved [as climate background state changed from warm conditions of the early](#)  
1310 [and middle Pliocene through the intensification of Northern Hemisphere glaciation during the](#)  
1311 [late Pliocene and Quaternary](#). [Understanding the](#) interactions of climate on orbital and  
1312 suborbital time scales will lead to a fuller understanding of the mechanisms responsible for the  
1313 Quaternary ice ages.

1314

#### 1315 **Data availability**

1316 All datasets and age models have been deposited with PANGAEA [and are available at](#)  
1317 <https://doi.org/10.1594/PANGAEA.951401> (Hodell, 2022).

1318

#### 1319 **Author contributions**

1320 DAH led the effort to drill Site U1385 and LL and DAH were shipboard scientists aboard IODP  
1321 Expedition 393 that recovered the cores. LL constructed the spliced composite section for Site  
1322 U1385. MJV provided taxonomic expertise and MJV and NT selected foraminifera and  
1323 prepared samples for stable isotope analysis. JER and JN operated the mass spectrometers and  
1324 produced the stable isotope data. LL, SJC and DAH oversaw the XRF analyses of the cores.  
1325 LCS, PCT and VM provided data and interpretation of Core MD01-2444. EWW advised on  
1326 the correlation of the marine sediment record to the Greenland and Antarctic ice cores. DAH,  
1327 PCT and EWW wrote the first draft and all authors contributed to the submitted manuscript.

1328

#### 1329 **Competing interests**

1330  
1331 Two of the (co-)authors are a member of the editorial board of *Climate of the Past*. The peer-  
1332 review process was guided by an independent editor, and the authors also have no other  
1333 competing interests to declare.

1334

#### 1335 **Disclaimer**

Deleted: One of the objectives of upcoming

Deleted: is to

Deleted: U1385

Deleted: to study

Deleted: during through the Quaternary and Pliocene

Deleted: (Hodell et al., 2022)

Deleted:

Deleted: these

Deleted:

Deleted: as "in review" and will be publically available when the paper is accepted and a DOI is issued

1347 Publisher's note: Copernicus Publications remains neutral with regard to jurisdictional claims  
1348 in published maps and institutional affiliations.

1349  
1350  
1351

#### 1352 **Acknowledgments**

1353 Samples were provided by the International Ocean Discovery Program (IODP). We thank the  
1354 IODP Expedition 393 drilling crew, ship's crew, and scientific and technical staff of the  
1355 drillship *JOIDES Resolution* without whom recovering Site U1385 would not have been  
1356 possible. We thank Jeannie Booth and Ian Mather for laboratory support. This research was  
1357 supported by the Natural Environmental Research Council Grants NE/J00653X/1,  
1358 NE/K005804/1, NE/J017922/1 and NE/R000204/1 and Leverhulme Trust Project RPG2014-  
1359 417.

1360  
1361  
1362

#### 1363 **References:**

1364 Ahn, J. and Brook, E. J.: Siple Dome ice reveals two modes of millennial CO<sub>2</sub> change  
1365 during the last ice age, *Nature Communications*, 5, 3723, doi:10.1038/ncomms4723,  
1366 URL <https://doi.org/10.1038/ncomms4723>, 2014.

1367

1368 [Ahn, S., Khider, D., Lisiecki, L. E., and Lawrence, C. E.: A probabilistic Pliocene-  
1369 Pleistocene stack of benthic δ18O using a profile hidden Markov model, \*Dynamics  
1370 and Statistics of the Climate System\*, 2, 1–16. <https://doi.org/10.1093/climsys/dzx002>,  
1371 2017.](#)

1372

1373 Alley, R. B.: Wally was right: Predictive ability of the North Atlantic “Conveyor Belt”  
1374 hypothesis for abrupt climate change, *Annual Review of Earth and Planetary  
1375 Sciences*, 35, 241–272, doi:10.1146/annurev.earth.35.081006.131524, URL  
1376 <https://doi.org/10.1146/annurev.earth.35.081006.131524>, 2007.

1377

1378 Alonso-Garcia, M., Sierro, F., Kucera, M., Flores, J., Cacho, I., and Andersen, N.: Ocean  
1379 circulation, ice sheet growth and inter-hemispheric coupling of millennial climate  
1380 variability during the mid-Pleistocene (ca 800–400ka), *Quaternary Science Reviews*,  
1381 30, 3234–3247, doi:<https://doi.org/10.1016/j.quascirev.2011.08.005>, URL  
1382 <https://www.sciencedirect.com/science/article/pii/S0277379111002435>, 2011.

1383

1384 Anderson, R. F., Ali, S., Bradtmiller, L. I., Nielsen, S. H. H., Fleisher, M. Q., Anderson, B.  
1385 E., and Burckle, H.: Wind-driven upwelling in the Southern Ocean and the deglacial  
1386 rise in atmospheric CO<sub>2</sub>, *Science*, 323, 1443–1448, doi:10.1126/science.1167441,  
1387 URL <https://www.science.org/doi/abs/10.1126/science.1167441>, 2009.

1388

1389 [Baggenstos, D., Häberli, M., and Schmitt, J.: Earth's radiative imbalance from the Last  
1390 Glacial Maximum to the present, \*Proc. Nat. Acad. Sci.\*, 116 \(30\), 14881–14886,  
1391 <https://doi.org/10.1073/pnas.1905447116>, 2019.](#)

1392  
1393  
1394 Bajo, P., Drysdale, R. N., Woodhead, J. D., Hellstrom, J. C., Hodell, D.A., Ferretti, P.,  
1395 Voelker, A. H. L., Zanchetta, G., Rodrigues, T., Wolff, E. W., Tyler, J., Frisia, S.,  
1396 Spotl, C., and Fallick, A. E.: Persistent influence of obliquity on ice age terminations  
1397 since the Middle Pleistocene transition, *Science*, 367, 1235–1239,  
1398 doi:10.1126/science.aaw1114, URL  
1399 https://www.science.org/doi/abs/10.1126/science.aaw1114, 2020.  
1400  
1401 Barker, S., Starr, A., van der Lubbe, J., Doughty, A., Knorr, G., Conn, S., Lordsmith, S.,  
1402 Owen, L., Nederbragt, A., Hemming, S., Hall, I., Levay, L., null null, Berke, M. A.,  
1403 Brentegani, L., Caley, T., Cartagena-Sierra, A., Charles, C. D., Coenen, J. J., Crespin,  
1404 J. G., Franzese, A. M., Gruetzner, J., Han, X., Hines, S. K. V., Espejo, F. J. J., Just, J.,  
1405 Koutsodendris, A., Kubota, K., Lathika, N., Norris, R. D., dos Santos, T. P.,  
1406 Robinson, R., Rolison, J. M., Simon, M. H., Tanguan, D., Yamane, M., and Zhang,  
1407 H.: Persistent influence of precession on northern ice sheet variability since the early  
1408 Pleistocene, *Science*, 376, 961–967, doi:10.1126/science.abm4033, URL  
1409 https://www.science.org/doi/abs/10.1126/science.abm4033, 2022.  
1410  
1411 Barker, S. and Knorr, G.: Millennial scale feedbacks determine the shape and rapidity of  
1412 glacial termination, *Nature Communications*, 12, 2273, doi:10.1038/s41467-021-  
1413 22388-6, 2021.  
1414  
1415 Barker, S., Knorr, G., Edwards, R., Parrenin, F., Putnam, A., Skinner, L., Wolff, E., and  
1416 Ziegler, M.: 800,000 years of abrupt climate variability, *Science*, 334, 347–51,  
1417 doi:10.1126/science.1203580, 2011.  
1418  
1419 Barker, S., Chen, J., Gong, X., Jonkers, L., Knorr, G., and Thornalley, D.: Icebergs not the  
1420 trigger for North Atlantic cold events, *Nature*, 520, 333–336,  
1421 doi:10.1038/nature14330, URL https://doi.org/10.1038/nature14330, 2015.  
1422  
1423 Barker, S., Zhang, X., Jonkers, L., Lordsmith, S., Conn, S., and Knorr, G.: Strengthening  
1424 Atlantic inflow across the mid- Pleistocene Transition, *Paleoceanography and*  
1425 *Paleoclimatology*, 36, e2020PA004 200, doi:https://doi.org/10.1029/2020PA004200,  
1426 URL https://agupubs.onlinelibrary.wiley.com/doi/abs/10.1029/2020PA004200,  
1427 e2020PA004200 2020PA004200, 2021.  
1428  
1429 Batchelor, C. L., Margold, M., Krapp, M., Murton, D. K., Dalton, A. S., Gibbard, P. L.,  
1430 Stokes, C. R., Murton, J. B., and Manica, A.: The configuration of Northern  
1431 Hemisphere ice sheets through the Quaternary, *Nature Communications*, 10, 3713,  
1432 doi:10.1038/s41467-019-11601-2, URL https://doi.org/10.1038/s41467-019-11601-2,  
1433 2019.  
1434  
1435 Bauska, T. K., Marcott, S. A., and Brook, E. J.: Abrupt changes in the global carbon cycle  
1436 during the last glacial period, *Nature Geoscience*, 14, 91–96, doi:10.1038/s41561-  
1437 020-00680-2, URL https://doi.org/10.1038/s41561-020-00680-2, 2021.  
1438  
1439 Bender, M., Sowers, T., Dickson, M.-L., Orchardo, J., Grootes, P., Mayewski, P. A., and  
1440 Meese, D. A.: Climate correlations between Greenland and Antarctica during the past

**Deleted:** Barker, Knorr, Edwards, Parrenin, Putnam, Skinner, Wolff, and Ziegler]

1443 100,000 years, *Nature*, 372, 663–666, doi:10.1038/372663a0, URL  
1444 <https://doi.org/10.1038/372663a0>, 1994.  
1445  
1446 Benzi, R., Parisi, G., Suter, A., and Vulpiani, A.: Stochastic resonance in climatic change,  
1447 *Tellus*, 34, 10–16, doi:<https://doi.org/10.1111/j.2153-3490.1982.tb01787.x>, 1982.  
1448  
1449 [Berends, C. J., Köhler, P., Lourens, L. J., and van de Wal, R. S. W.: On the cause of the mid-](#)  
1450 [Pleistocene transition, \*Reviews of Geophysics\*, 59, e2020RG000727.](#)  
1451 <https://doi.org/10.1029/2020RG000727>, 2021.  
1452  
1453  
1454 Berger, A., Loutre, M. F., and Melice, J. L.: Equatorial insolation: from precession harmonics  
1455 to eccentricity frequencies, *Climate of the Past*, 2, 131–136, doi:10.5194/cp-2-131-  
1456 2006, URL <https://cp.copernicus.org/articles/2/131/2006/>, 2006.  
1457 [Berger, A., Loutre, M.-F., and Yin, Q.: Total irradiation during any time interval of the year](#)  
1458 [using elliptic integrals, \*Quaternary Science Reviews\*, 29, 1968-1982.](#)  
1459 <https://doi.org/10.1016/j.quascirev.2010.05.007>, 2010.  
1460  
1461 Billups, K. and Scheinwald, A.: Origin of millennial-scale climate signals in the subtropical  
1462 North Atlantic, *Paleo-oceanography*, 29, doi:10.1002/2014PA002641, 2014.  
1463  
1464 Birner, B., Hodell, D. A., Tzedakis, P. C., and Skinner, L. C.: Similar millennial climate  
1465 variability on the Iberian margin during two early Pleistocene glacials and MIS 3,  
1466 *Paleoceanography*, 31, 203–217, doi:<https://doi.org/10.1002/2015PA002868>, URL  
1467 <https://agupubs.onlinelibrary.wiley.com/doi/abs/10.1002/2015PA002868>, 2016.  
1468  
1469 Blunier, T. and Brook, E. J.: Timing of millennial-scale climate change in Antarctica and  
1470 Greenland during the Last Glacial Period, *Science*, 291, 109–112,  
1471 doi:10.1126/science.291.5501.109, URL  
1472 <https://www.science.org/doi/abs/10.1126/science.291.5501.109>, 2001.  
1473  
1474 Bolton, C. T., Bailey, I., Friedrich, O., Tachikawa, K., de Garidel-Thoron, T., Vidal, L.,  
1475 Sonzogni, C., Marino, G., Rohling, E. J., Robinson, M. M., Ermini, M., Koch, M.,  
1476 Cooper, M. J., and Wilson, P. A.: North Atlantic midlatitude surface-circulation  
1477 changes through the Plio-Pleistocene intensification of Northern Hemisphere  
1478 Glaciation, *Paleoceanography and Paleoclimatology*, 33, 1186–1205,  
1479 doi:<https://doi.org/10.1029/2018PA003412>, URL  
1480 <https://agupubs.onlinelibrary.wiley.com/doi/abs/10.1029/2018PA003412>, 2018.  
1481  
1482 Bond, G., Heinrich, H., Broecker, W., Labeyrie, L., McManus, J., Andrews, J., Huon, S.,  
1483 Jantschik, R., Clasen, S., Simet, C., Tedesco, K., Klas, M., Bonani, G., and Ivy,  
1484 S.: Evidence for massive discharges of icebergs into the North Atlantic ocean during  
1485 the last glacial period, *Nature*, 360, 245–249, doi:10.1038/360245a0, URL  
1486 <https://doi.org/10.1038/360245a0>, 1992.  
1487  
1488 Bond, G., Broecker, W., Johnsen, S., McManus, J., Labeyrie, L., Jouzel, J., and Bonani, G.:  
1489 Correlations between climate records from North Atlantic sediments and Greenland  
1490 ice, *Nature*, 365, 143–147, doi:10.1038/365143a0, URL  
1491 <https://doi.org/10.1038/365143a0>, 1993.  
1492

Formatted: English (UK)

Deleted: ¶

- 1494 Broecker, W., Bond, G., Klas, M., Clark, E., and McManus, J.: Origin of the northern  
 1495 Atlantic's Heinrich events, *Climate Dynamics*, 6, 265–273, doi:10.1007/BF00193540,  
 1496 URL <https://doi.org/10.1007/BF00193540>, 1992.  
 1497
- 1498 Broecker, W. S. and van Donk, J.: Insolation changes, ice volumes, and the O18 record in  
 1499 deep-sea cores, *Reviews of Geophysics*, 8, 169–198,  
 1500 doi:<https://doi.org/10.1029/RG008i001p00169>, URL  
 1501 <https://agupubs.onlinelibrary.wiley.com/doi/abs/10.1029/RG008i001p00169>, 1970.  
 1502
- 1503 Broecker, W. S., Bond, G., Klas, M., Bonani, G., and Wolfli, W.: A salt oscillator in the  
 1504 glacial Atlantic? 1. The concept, *Paleoceanography*, 5, 469–477,  
 1505 doi:<https://doi.org/10.1029/PA005i004p00469>, URL  
 1506 <https://agupubs.onlinelibrary.wiley.com/doi/abs/10.1029/PA005i004p00469>, 1990.  
 1507
- 1508 Brown, N. and Galbraith, E. D.: Hosed vs. unhosed: interruptions of the Atlantic Meridional  
 1509 Overturning Circulation in a global coupled model, with and without freshwater  
 1510 forcing, *Climate of the Past*, 12, 1663–1679, doi:10.5194/cp-12-1663-2016, URL  
 1511 <https://cp.copernicus.org/articles/12/1663/2016/>, 2016.  
 1512
- 1513 Buizert, C. and Schmittner, A.: Southern Ocean control of glacial AMOC stability and  
 1514 Dansgaard-Oeschger interstadial duration, *Paleoceanography*, 30, 1595–1612,  
 1515 doi:<https://doi.org/10.1002/2015PA002795>, URL  
 1516 <https://agupubs.onlinelibrary.wiley.com/doi/abs/10.1002/2015PA002795>, 2015.  
 1517
- 1518 Burns, S. J., Welsh, L. K., Scroxton, N., Cheng, H., and Edwards, R. L.: Millennial  
 1519 and orbital scale variability of the South American Monsoon during the penultimate  
 1520 glacial period, *Scientific Reports*, 9, 1234, doi:10.1038/s41598-018-37854-3, URL  
 1521 <https://doi.org/10.1038/s41598-018-37854-3>, 2019.  
 1522
- 1523 Chalk, T. B., Hain, M. P., Foster, G. L., Rohling, E. J., Sexton, P. F., Badger, M. P. S.,  
 1524 Cherry, S. G., Hasenfratz, A. P., Haug, G. H., Jaccard, S. L., Martinez-Garcia, A.,  
 1525 Palike, H., Pancost, R. D., and Wilson, P. A.: Causes of ice age intensification across  
 1526 the Mid-Pleistocene Transition, *Proceedings of the National Academy of Sciences*,  
 1527 114, 13,114–13,119, doi:10.1073/pnas.1702143114, URL  
 1528 <https://www.pnas.org/doi/abs/10.1073/pnas.1702143114>, 2017.  
 1529
- 1530 Channell, J., Hodell, D., Romero, O., Hillaire-Marcel, C., de Vernal, A., Stoner, J., Mazaud,  
 1531 A., and Rohl, U.: A 750-kyr detrital-layer stratigraphy for the North Atlantic (IODP  
 1532 Sites U1302–U1303, Orphan Knoll, Labrador Sea), *Earth and Planetary Science  
 1533 Letters*, 317–318, 218–230, doi:<https://doi.org/10.1016/j.epsl.2011.11.029>, URL  
 1534 <https://www.sciencedirect.com/science/article/pii/S0012821X11006868>, 2012.  
 1535
- 1536 Channell, J., Hodell, D., Crowhurst, S., Skinner, L., and Muscheler, R.: Relative  
 1537 paleointensity (RPI) in the latest Pleistocene (10–45 ka) and implications for  
 1538 deglacial atmospheric radiocarbon, *Quaternary Science Reviews*, 191, 57–72,  
 1539 doi:<https://doi.org/10.1016/j.quascirev.2018.05.007>, URL  
 1540 <https://www.sciencedirect.com/science/article/pii/S0277379118302828>, 2018.  
 1541
- 1542 Clark, P. U., Archer, D., Pollard, D., Blum, J. D., Rial, J. A., Brovkin, V., Mix, A. C., Pisias,  
 1543 N. G., and Roy, M.: The middle Pleistocene transition: characteristics, mechanisms,



1544 and implications for long-term changes in atmospheric pCO<sub>2</sub>, *Quaternary Science*  
1545 *Reviews*, 25, 3150–3184, doi:<https://doi.org/10.1016/j.quascirev.2006.07.008>, URL  
1546 <https://www.sciencedirect.com/science/article/pii/S0277379106002332>, critical  
1547 *Quaternary Stratigraphy*, 2006.  
1548

1549 Dansgaard, W., Clausen, H. B., Gundestrup, N., Hammer, C. U., Johnsen, S. F.,  
1550 Kristinsdottir, P. M., and Reeh, N.: A new Greenland deep ice core, *Science*, 218,  
1551 1273–1277, doi:[10.1126/science.218.4579.1273](https://doi.org/10.1126/science.218.4579.1273), URL  
1552 <https://www.science.org/doi/abs/10.1126/science.218.4579.1273>, 1982.  
1553

1554 DeBoer, A. M. and Nof, D.: The Bering Strait's grip on the northern hemisphere climate,  
1555 *Deep Sea Research Part I: Oceanographic Research Papers*, 51, 1347–1366,  
1556 doi:<https://doi.org/10.1016/j.dsr.2004.05.003>, URL  
1557 <https://www.sciencedirect.com/science/article/pii/S0967063704000901>, 2004.  
1558

1559 de Verdier, A. C.: A simple model of millennial oscillations of the thermohaline circulation,  
1560 *Journal of Physical Oceanography*, 37, 1142–1155, doi:[10.1175/JPO3056.1](https://doi.org/10.1175/JPO3056.1), URL  
1561 <https://journals.ametsoc.org/view/journals/phoc/37/5/jpo3056.1.xml>, 2007.  
1562

1563 Dokken, T. M., Nisancioglu, K. H., Li, C., Battisti, D. S., and Kissel, C.: Dansgaard-  
1564 Oeschger cycles: Interactions between ocean and sea ice intrinsic to the Nordic seas,  
1565 *Paleoceanography*, 28, 491–502, doi:<https://doi.org/10.1002/palo.20042>, URL  
1566 <https://agupubs.onlinelibrary.wiley.com/doi/abs/10.1002/palo.20042>, 2013.  
1567

1568 Duplessy, J.-C., Labeyrie, L., and Waelbroeck, C.: Constraints on the ocean  
1569 oxygen isotopic enrichment between the Last Glacial Maximum and the  
1570 Holocene: Paleoceanographic implications, *Quaternary Science Reviews*,  
1571 21, 315–330, doi:[https://doi.org/10.1016/S0277-3791\(01\)00107-X](https://doi.org/10.1016/S0277-3791(01)00107-X), URL  
1572 <https://www.sciencedirect.com/science/article/pii/S027737910100107X>,  
1573 *ePILOG*, 2002.  
1574

1575 Dyez, K. A., Honisch, B., and Schmidt, G. A.: Early Pleistocene obliquity-scale pCO<sub>2</sub>  
1576 variability at 1.5 million years ago, *Paleoceanography and Paleoclimatology*, 33,  
1577 1270–1291, doi:<https://doi.org/10.1029/2018PA003349>, URL  
1578 <https://agupubs.onlinelibrary.wiley.com/doi/abs/10.1029/2018PA003349>, 2018.  
1579

1580 Elderfield, H., Ferretti, P., Greaves, M., Crowhurst, S., McCave, I. N., Hodell, D., and  
1581 Piotrowski, A. M.: Evolution of ocean temperature and ice volume through the Mid-  
1582 Pleistocene Climate Transition, *Science*, 337, 704–709, doi:[10.1126/science.1221294](https://doi.org/10.1126/science.1221294),  
1583 URL <https://www.science.org/doi/abs/10.1126/science.1221294>, 2012.  
1584

1585 EPICA Community Members: Eight glacial cycles from an Antarctic ice core, *Nature*, 429,  
1586 623–628, doi:[10.1038/nature02599](https://doi.org/10.1038/nature02599), URL <https://doi.org/10.1038/nature02599>, 2004.  
1587

1588 Ferretti, P., Crowhurst, S. J., Naafs, B. D. A., and Barbante, C.: The Marine Isotope Stage 19  
1589 in the mid-latitude North Atlantic Ocean: astronomical signature and intra-interglacial  
1590 variability, *Quaternary Science Reviews*, 108, 95–110,  
1591 doi:<https://doi.org/10.1016/j.quascirev.2014.10.024>, URL  
1592 <https://www.sciencedirect.com/science/article/pii/S0277379114004119>, 2015.  
1593

- 1594 Friedrich, T., Timmermann, A., Menviel, L., Elison Timm, O., Mouchet, A., and Roche,  
1595 D. M.: The mechanism behind internally generated centennial-to-millennial scale  
1596 climate variability in an earth system model of intermediate complexity,  
1597 *Geoscientific Model Development*, 3, 377–389, doi:10.5194/gmd-3-377-2010,  
1598 URL <https://gmd.copernicus.org/articles/3/377/2010/>, 2010.  
1599
- 1600 Galaasen, E., Ninnemann, U., Kessler, A., Irvah, N., Rosenthal, Y., Tjiputra, J., Bouttes, N.,  
1601 Roche, D., Kleiven, K. H., and Hodell, D.: Interglacial instability of North Atlantic  
1602 Deep Water ventilation, *Science*, 367, 1485–1489, doi:10.1126/science.aay6381,  
1603 2020.  
1604
- 1605 Galaasen, E. V., Ninnemann, U. S., Irvah, N., Kleiven, H. K. F., Rosenthal, Y., Kissel, C.,  
1606 and Hodell, D. A.: Rapid reductions in North Atlantic Deep Water during the peak of  
1607 the last interglacial period, *Science*, 343, 1129–1132, doi:10.1126/science.1248667,  
1608 URL <https://www.science.org/doi/abs/10.1126/science.1248667>, 2014.  
1609
- 1610 Galbraith, E. D. and de Lavergne, C.: Response of a comprehensive climate model to a broad  
1611 range of external forcings: relevance for deep ocean ventilation and the development  
1612 of late Cenozoic ice ages, *Climate Dynamics*, 52, 653–679, 2018.  
1613
- 1614 Ganopolski, A. and Rahmstorf, S.: Rapid changes of glacial climate simulated in a  
1615 coupled climate model, *Nature*, 409, 153–158, doi:10.1038/35051500, URL  
1616 <https://doi.org/10.1038/35051500>, 2001.  
1617
- 1618 Gebbie, G.: Tracer transport timescales and the observed Atlantic-Pacific lag in the timing of  
1619 the Last Termination, *Paleoceanography*, 27,  
1620 doi:<https://doi.org/10.1029/2011PA002273>, URL  
1621 <https://agupubs.onlinelibrary.wiley.com/doi/abs/10.1029/2011PA002273>,  
1622 2012.  
1623
- 1624 Gildor, H. and Tziperman, E.: A sea ice climate switch mechanism for the 100-kyr glacial  
1625 cycles, *Journal of Geophysical Research*, 106, doi:10.1029/1999JC000120, 2001.  
1626
- 1627 Gottschalk, J., Skinner, L. C., Jaccard, S. L., Menviel, L., Nehrass-  
1628 Ahles, C., and Waelbroeck, C.: Southern Ocean link between changes  
1629 in atmospheric CO<sub>2</sub> levels and northern-hemisphere climate anomalies  
1630 during the last two glacial periods, *Quaternary Science Reviews*, 230, 106 067,  
1631 doi:<https://doi.org/10.1016/j.quascirev.2019.106067>, URL  
1632 <https://www.sciencedirect.com/science/article/pii/S0277379118310461>, 2020  
1633
- 1634 Grutzner, J. and Higgins, S. M.: Threshold behavior of millennial scale variability in deep  
1635 water hydrography inferred from a 1.1 Ma long record of sediment provenance at the  
1636 southern Gardar Drift, *Paleoceanography*, 25,  
1637 doi:<https://doi.org/10.1029/2009PA001873>, URL  
1638 <https://agupubs.onlinelibrary.wiley.com/doi/abs/10.1029/2009PA001873>, 2010.  
1639
- 1640 Haerberli, M., Baggenstos, D., Schmitt, J., Grimmer, M., Michel, A., Kellerhals, T., and  
1641 Fischer, H.: Snapshots of mean ocean temperature over the last 700 000 years using  
1642 noble gases in the EPICA Dome C ice core, *Climate of the Past*, 17, 843–867,

Deleted: [Gottschalk, Skinner, Jaccard, Menviel, Nehrass-Ahles, and Waelbroeck]

Deleted: [

1647 doi:10.5194/cp-17-843-2021, URL <https://cp.copernicus.org/articles/17/843/2021/>,  
1648 2021.  
1649  
1650 Hagelberg, T. K., Bond, G., and deMenocal, P.: Milankovitch band forcing of sub-  
1651 Milankovitch climate variability during the Pleistocene, *Paleoceanography*, 9, 545–  
1652 558, doi:<https://doi.org/10.1029/94PA00443>, URL  
1653 <https://agupubs.onlinelibrary.wiley.com/doi/abs/10.1029/94PA00443>, 1994.  
1654  
1655 Heinrich, H.: Origin and consequences of cyclic ice rafting in the Northeast Atlantic Ocean  
1656 during the past 130,000 years, *Quaternary Research*, 29, 142–152,  
1657 doi:[https://doi.org/10.1016/0033-5894\(88\)90057-9](https://doi.org/10.1016/0033-5894(88)90057-9), URL  
1658 <https://www.sciencedirect.com/science/article/pii/0033589488900579>, 1988.  
1659  
1660 Hemming, S. R.: Heinrich events: Massive late Pleistocene detritus layers of the North  
1661 Atlantic and their global climate imprint, *Reviews of Geophysics*, 42,  
1662 doi:<https://doi.org/10.1029/2003RG000128>, URL  
1663 <https://agupubs.onlinelibrary.wiley.com/doi/abs/10.1029/2003RG000128>, 2004.  
1664  
1665 Henry, L. G., McManus, J. F., Curry, W. B., Roberts, N. L., Piotrowski, A. M., and  
1666 Keigwin, L. D.: North Atlantic ocean circulation and abrupt climate change during  
1667 the last glaciation, *Science*, 353, 470–474, doi:10.1126/science.aaf5529, URL  
1668 <https://www.science.org/doi/abs/10.1126/science.aaf5529>, 2016.  
1669  
1670 Higgins, J. A., Kurbatov, A. V., Spaulding, N. E., Brook, E., Introne, D. S., Chimiak, L. M.,  
1671 Yan, Y., Mayewski, P. A., and Bender, M. L.: Atmospheric composition 1 million  
1672 years ago from blue ice in the Allan Hills, Antarctica, *Proceedings of the National  
1673 Academy of Sciences*, 112, 6887–6891, doi:10.1073/pnas.1420232112, URL  
1674 <https://www.pnas.org/doi/abs/10.1073/pnas.1420232112>, 2015.  
1675  
1676 Hinnov, L. A., Schulz, M., and Yiou, P.: Interhemispheric space–time attributes of the  
1677 Dansgaard–Oeschger oscillations between 100 and 0 ka, *Quaternary Science  
1678 Reviews*, 21, 1213–1228, doi:[https://doi.org/10.1016/S0277-3791\(01\)00140-8](https://doi.org/10.1016/S0277-3791(01)00140-8), URL  
1679 <https://www.sciencedirect.com/science/article/pii/S0277379101001408>,  
1680 2002.  
1681  
1682 [Hodell, D. A. \(2022\): Benthic and planktonic oxygen and carbon isotopes and XRF data at  
1683 IODP Site U1385 and core MD01-2444 from 0 to 1.5  
1684 Ma. PANGAEA, <https://doi.org/10.1594/PANGAEA.951401>](#)  
1685  
1686 [Hodell, D.A., Abrantes, F., Alvarez Zarikian, C.A., and the Expedition 397 Scientists:  
1687 Expedition 397 Preliminary Report: Iberian Margin Paleoclimate. International  
1688 Ocean Discovery Program. \[https://doi.org/10.14379/iodp.pr.397.2023\\\_2023\]\(https://doi.org/10.14379/iodp.pr.397.2023\_2023\).](#)  
1689  
1690 Hodell, D., Crowhurst, S., Skinner, L., Tzedakis, P. C., Margari, V., Channell, J. E.,  
1691 Kamenov, G., Maclachlan, S., and Rothwell, G.: Response of Iberian Margin  
1692 sediments to orbital and suborbital forcing over the past 420ka, *Paleoceanography*,  
1693 28, 185–199, doi:<https://doi.org/10.1002/palo.20017>, URL  
1694 <https://agupubs.onlinelibrary.wiley.com/doi/abs/10.1002/palo.20017>, 2013.  
1695

**Deleted:** Hilborn, R. C. and Sprott, J. C.: Chaos and Nonlinear Dynamics: An Introduction for Scientists and Engineers, *American Journal of Physics*, 62, 861–862, doi:10.1119/1.17477, URL <https://doi.org/10.1119/1.17477>, 1994.

Hinnov, L.A., Schulz, M., and Yiou, P.: Interhemispheric space–time attributes of the Dansgaard–Oeschger oscillations between 100 and 0 ka, *Quaternary Science Reviews*, 21, 1213–1228, 2002.

**Formatted:** Font: Times

**Formatted:** Font: (Default) Times New Roman, 12 pt, Font colour: Text 1

**Formatted:** Indent: Left: 0 cm, Hanging: 1.27 cm

**Formatted:** Font: (Default) Times New Roman, 12 pt, Italic, Font colour: Text 1

**Formatted:** Font: (Default) Times New Roman, 12 pt, Font colour: Text 1

**Formatted:** Font: (Default) Times New Roman, 12 pt, Font colour: Text 1

**Formatted:** Font: (Default) Times New Roman, 12 pt, Font colour: Text 1

**Deleted:** Hodell, D.A., Abrantes, F., and Alvarez Zarikian, C.A.: *Expedition 397 Scientific Prospectus: Iberian Margin Paleoclimate. International Ocean Discovery Program.* [https://doi.org/10.14379/iodp.sp.397.2022\\_2022](https://doi.org/10.14379/iodp.sp.397.2022_2022).

- 1712 Hodell, D., Lourens, L., Crowhurst, S., Konijnendijk, T., Tjallingii, R., Jimenez-Espejo, F.,  
1713 Skinner, L., Tzedakis, P., Abrantes, F., Acton, G. D., Alvarez Zarikian, C. A., Bahr,  
1714 A., Balestra, B., Barranco, E. L., Carrara, G., Ducassou, E., Flood, R. D., Flores, J.-  
1715 A., Furota, S., Grimalt, J., Grunert, P., Hernandez-Molina, J., Kim, J. K., Krissek, L.  
1716 A., Kuroda, J., Li, B., Lofi, J., Margari, V., Martrat, B., Miller, M. D., Nanayama, F.,  
1717 Nishida, N., Richter, C., Rodrigues, T., Rodriguez-Tovar, F. J., Roque, A. C. F.,  
1718 Sanchez Goni, M. F., Sierro Sanchez, F. J., Singh, A. D., Sloss, C. R., Stow, D. A.,  
1719 Takashimizu, Y., Tzanova, A., Voelker, A., Xuan, C., and Williams, T.: A reference  
1720 time scale for Site U1385 (Shackleton Site) on the SW Iberian Margin, *Global*  
1721 *and Planetary Change*, 133, 49–64,  
1722 doi:<https://doi.org/10.1016/j.gloplacha.2015.07.002>, URL  
1723 <https://www.sciencedirect.com/science/article/pii/S0921818115001423>, 2015.  
1724
- 1725 Hodell, D. A. and Channell, J. E. T.: Mode transitions in Northern Hemisphere glaciation:  
1726 co-evolution of millennial and orbital variability in Quaternary climate, *Climate of the*  
1727 *Past*, 12, 1805–1828, doi:10.5194/cp-12-1805-2016, URL  
1728 <https://cp.copernicus.org/articles/12/1805/2016/>, 2016.  
1729
- 1730 Hodell, D. A., Channell, J. E. T., Curtis, J. H., Romero, O. E., and Rohl, U.: Onset of  
1731 “Hudson Strait” Heinrich events in the eastern North Atlantic at the end of the middle  
1732 Pleistocene transition (640 ka)?, *Paleoceanography*, 23,  
1733 doi:<https://doi.org/10.1029/2008PA001591>, URL  
1734 <https://agupubs.onlinelibrary.wiley.com/doi/abs/10.1029/2008PA001591>, 2008.  
1735
- 1736 Hodell, D. A., Minth, E. K., Curtis, J. H., McCave, I. N., Hall, I. R., Channell, J. E., and  
1737 Xuan, C.: Surface and deep-water hydrography on Gardar Drift (Iceland Basin)  
1738 during the last interglacial period, *Earth and Planetary Science Letters*, 288, 10–19,  
1739 doi:<https://doi.org/10.1016/j.epsl.2009.08.040>, URL  
1740 <https://www.sciencedirect.com/science/article/pii/S0012821X09005147>, 2009.  
1741
- 1742 Honisch, B., Ridgwell, A., Schmidt, D. N., Thomas, E., Gibbs, S. J., Sluijs, A., Zeebe, R.,  
1743 Kump, L., Martindale, R. C., Greene, S. E., Kiessling, W., Ries, J., Zachos, J. C.,  
1744 Royer, D. L., Barker, S., Marchitto, T. M., Moyer, R., Pelejero, C., Ziveri, P.,  
1745 Foster, G. L., and Williams, B.: The geological record of ocean acidification, *Science*,  
1746 335, 1058–1063, doi:10.1126/science.1208277, URL  
1747 <https://www.science.org/doi/abs/10.1126/science.1208277>, 2012.  
1748
- 1749 Hoogakker, B., Elderfield, H., Oliver, K., and Crowhurst, S.: Benthic  
1750 foraminiferal oxygen isotope offsets over the last glacial-interglacial cycle,  
1751 *Paleoceanography*, 25, doi:<https://doi.org/10.1029/2009PA001870>, URL  
1752 <https://agupubs.onlinelibrary.wiley.com/doi/abs/10.1029/2009PA001870>, 2010.  
1753
- 1754 Hu, A., Meehl, G. A., Han, W., Abe-Ouchi, A., Morrill, C., Okazaki, Y., and Chikamoto,  
1755 M. O.: The Pacific-Atlantic seesaw and the Bering Strait, *Geophysical Research*  
1756 *Letters*, 39, doi:<https://doi.org/10.1029/2011GL050567>, URL  
1757 <https://agupubs.onlinelibrary.wiley.com/doi/abs/10.1029/2011GL050567>, 2012a.  
1758
- 1759 Hu, A., Meehl, G. A., Han, W., Timmermann, A., Otto-Bliesner, B., Liu, Z., Washington, W.  
1760 M., Large, W., Abe-Ouchi, A., Kimoto, M., Lambeck, K., and Wu, B.: Role of  
1761 the Bering Strait on the hysteresis of the ocean conveyor belt circulation and glacial

1762 climate stability, *Proceedings of the National Academy of Sciences*, 109, 6417–6422,  
 1763 doi:10.1073/pnas.1116014109, URL  
 1764 <https://www.pnas.org/doi/abs/10.1073/pnas.1116014109>, 2012b.  
 1765  
 1766 Huybers, P. and Curry, W.: Links between annual, Milankovitch and continuum temperature  
 1767 variability, *Nature*, 441, 329–332, doi:10.1038/nature04745, URL  
 1768 <https://doi.org/10.1038/nature04745>, 2006.  
 1769  
 1770 Huybers, P. and Wunsch, C.: A depth-derived Pleistocene age model: Uncertainty estimates,  
 1771 sedimentation variability, and nonlinear climate change, *Paleoceanography*, 19,  
 1772 doi:<https://doi.org/10.1029/2002PA000857>, URL  
 1773 <https://agupubs.onlinelibrary.wiley.com/doi/abs/10.1029/2002PA000857>,  
 1774 2004.  
 1775  
 1776 Jansen, M. F., Nadeau, L.-P., and Merlis, T. M.: Transient versus equilibrium response of the  
 1777 ocean's overturning circulation to warming, *Journal of Climate*, 31, 5147 – 5163,  
 1778 doi:10.1175/JCLI-D-17-0797.1, URL  
 1779 <https://journals.ametsoc.org/view/journals/clim/31/13/jcli-d-17-0797.1.xml>, 2018.  
 1780  
 1781 Jouzel, J., Masson-Delmotte, V., Cattani, O., Dreyfus, G., Falourd, S., Hoffmann, G.,  
 1782 Minster, B., Nouet, J., Barnola, J. M., Chappellaz, J., Fischer, H., Gallet, J. C.,  
 1783 Johnsen, S., Leuenberger, M., Loulergue, L., Luethi, D., Oerter, H., Parrenin, F.,  
 1784 Raisbeck, G., Raynaud, D., Schilt, A., Schwander, J., Selmo, E., Souchez, R.,  
 1785 Spahni, R., Stauffer, B., Steffensen, J. P., Stenni, B., Stocker, T. F., Tison, J. L.,  
 1786 Werner, M., and Wolff, E. W.: Orbital and millennial Antarctic climate variability  
 1787 over the past 800,000 years, *Science*, 317, 793–796, doi:10.1126/science.1141038,  
 1788 URL <https://www.science.org/doi/abs/10.1126/science.1141038>, 2007.  
 1789  
 1790 Kawamura, K., Abe-Ouchi, A., Motoyama, H., Ageta, Y., Aoki, S., Azuma, N., Fujii, Y.,  
 1791 Fujita, K., Fujita, S., Fukui, K., Furukawa, T., Furusaki, A., Goto-Azuma, K.,  
 1792 Greve, R., Hirabayashi, M., Hondoh, T., Hori, A., Horikawa, S., Horiuchi, K.,  
 1793 Igarashi, M., Iizuka, Y., Kameda, T., Kanda, H., Kohno, M., Kuramoto, T., Matsushi,  
 1794 Y., Miyahara, M., Miyake, T., Miyamoto, A., Nagashima, Y., Nakayama, Y.,  
 1795 Nakazawa, T., Nakazawa, F., Nishio, F., Obinata, I., Ohgaito, R., Oka, A., Okuno,  
 1796 J., Okuyama, J., Oyabu, I., Parrenin, F., Pattyn, F., Saito, F., Saito, T., Saito, T.,  
 1797 Sakurai, T., Sasa, K., Seddik, H., Shibata, Y., Shinbori, K., Suzuki, K., Suzuki, T.,  
 1798 Takahashi, A., Takahashi, K., Takahashi, S., Takata, M., Tanaka, Y., Uemura, R.,  
 1799 Watanabe, G., Watanabe, O., Yamasaki, T., Yokoyama, K., Yoshimori, M., and  
 1800 Yoshimoto, T.: State dependence of climatic instability over the past 720,000 years  
 1801 from Antarctic ice cores and climate modeling, *Science Advances*, 3, e1600 446,  
 1802 doi:10.1126/sciadv.1600446, URL  
 1803 <https://www.science.org/doi/abs/10.1126/sciadv.1600446>, 2017.  
 1804  
 1805 Kleppin, H., Jochum, M., Otto-Bliesner, B., Shields, C. A., and Yeager, S.: Stochastic  
 1806 atmospheric forcing as a cause of Greenland climate transitions, *Journal of Climate*,  
 1807 28, 7741–7763, doi:10.1175/JCLI-D-14-00728.1, URL  
 1808 <https://journals.ametsoc.org/view/journals/clim/28/19/jcli-d-14-00728.1.xml>, 2015.  
 1809  
 1810 [Konijnendijk, T.Y.M., Ziegler, M., Lourens, L.J.: On the timing and forcing mechanisms of](#)  
 1811 [late Pleistocene glacial terminations: Insights from a new high-resolution benthic](#)

Deleted:

- 1813 [stable oxygen isotope record of the eastern Mediterranean, \*Quaternary Science\*](#)  
1814 [Reviews, 129, 308–320, <https://doi.org/10.1016/j.quascirev.2015.10.005>, 2015.](#)  
1815
- 1816 Larrasoana, J., Roberts, A., Rohling, E., Winkelhofer, M., and Wehausen, R.: Three million  
1817 years of monsoon variability over the northern Sahara, *Climate Dynamics*, 21, 689–  
1818 698, doi:10.1007/s00382-003-0355-z, 2003.  
1819
- 1820 Li, C., Battisti, D. S., Schrag, D. P., and Tziperman, E.: Abrupt climate shifts in Greenland  
1821 due to displacements of the sea ice edge, *Geophysical Research Letters*, 32,  
1822 doi:<https://doi.org/10.1029/2005GL023492>, URL  
1823 <https://agupubs.onlinelibrary.wiley.com/doi/abs/10.1029/2005GL023492>, 2005.  
1824
- 1825 Li, C., Battisti, D. S., and Bitz, C. M.: Can North Atlantic sea ice anomalies account for  
1826 Dansgaard–Oeschger climate signals?, *Journal of Climate*, 23, 5457–5475,  
1827 doi:10.1175/2010JCLI3409.1, URL  
1828 <https://journals.ametsoc.org/view/journals/clim/23/20/2010jcli3409.1.xml>, 2010.  
1829
- 1830 Li, M., Hinnov, L., and Kump, L.: Acycle: Time-series analysis software for paleoclimate  
1831 research and education, *Computers Geosciences*, 127, 12–22, doi:  
1832 10.1016/j.cageo.2019.02.011, 2019.  
1833
- 1834 Liautaud, P. R., Hodell, D. A., and Huybers, P. J.: Detection of significant climatic  
1835 precession variability in early Pleistocene glacial cycles, *Earth and Planetary*  
1836 *Science Letters*, 536, 116–137, doi:<https://doi.org/10.1016/j.epsl.2020.116137>, URL  
1837 <https://www.sciencedirect.com/science/article/pii/S0012821X20300807>, 2020.  
1838
- 1839 Liebrand, D. and de Bakker, A. T. M.: Bispectra of climate cycles show how ice ages are  
1840 fuelled, *Climate of the Past*, 15, 1959–1983, doi:10.5194/cp-15-1959-2019, URL  
1841 <https://cp.copernicus.org/articles/15/1959/2019/>, 2019.  
1842
- 1843 Lisiecki, L. E. and Raymo, M. E.: A Pliocene–Pleistocene stack of 57 globally distributed  
1844 benthic  $\delta^{18}\text{O}$  records, *Paleoceanography*, 20,  
1845 doi:<https://doi.org/10.1029/2004PA001071>, URL  
1846 <https://agupubs.onlinelibrary.wiley.com/doi/abs/10.1029/2004PA001071>,  
1847 2005.  
1848
- 1849 Liu, J., Mao, J., Huang, B., and Liu, P.: Chaos and reverse transitions in stochastic  
1850 resonance, *Physics Letters A*, 382, 3071–3078,  
1851 doi:<https://doi.org/10.1016/j.physleta.2018.08.016>, URL  
1852 <https://www.sciencedirect.com/science/article/pii/S0375960118308880>, 2018.  
1853
- 1854 Louergue, L., Schilt, A., Spahni, R., Masson-Delmotte, V., Blunier, T., Lemieux, B.,  
1855 Barnola, J.-M., Raynaud, D., Stocker, T. F., and Chappellaz, J.: Orbital and  
1856 millennial-scale features of atmospheric  $\text{CH}_4$  over the past 800,000 years, *Nature*,  
1857 453, 383–386, doi:10.1038/nature06950, URL <https://doi.org/10.1038/nature06950>,  
1858 2008.  
1859
- 1860 Lourens, L. J., Becker, J., Bintanja, R., Hilgen, F. J., Tuenter, E., van de Wal, R. S., and  
1861 Ziegler, M.: Linear and non-linear response of late Neogene glacial cycles to  
1862 obliquity forcing and implications for the Milankovitch theory, *Quaternary Science*

1863           Reviews, 29, 352–365, doi:<https://doi.org/10.1016/j.quascirev.2009.10.018>, URL  
1864           <https://www.sciencedirect.com/science/article/pii/S0277379109003631>, 2010.  
1865  
1866   Luthi, D., Le Floch, M., Bereiter, B., Blunier, T., Barnola, J.-M., Siegenthaler, U., Raynaud,  
1867   D., Jouzel, J., Fischer, H., Kawamura, K., and Stocker, T. F.: High-resolution carbon  
1868   dioxide concentration record 650,000–800,000 years before present, *Nature*, 453,  
1869   379–382, doi: 10.1038/nature06949, URL <https://doi.org/10.1038/nature06949>, 2008.  
1870  
1871   Lynch-Stieglitz, J.: The Atlantic meridional overturning circulation and abrupt climate  
1872   change, *Annual Review of Marine Science*, 9, 83–104, doi:10.1146/annurev-marine-  
1873   010816-060415, URL <https://doi.org/10.1146/annurev-marine-010816-060415>,  
1874   pMID: 27814029, 2017.  
1875  
1876   Mangerud, J.: The discovery of the Younger Dryas, and comments on the current meaning  
1877   and usage of the term, *Boreas*, 50, 1–5, doi:<https://doi.org/10.1111/bor.12481>, URL  
1878   <https://onlinelibrary.wiley.com/doi/abs/10.1111/bor.12481>, 2021.  
1879  
1880   Mantsis, D. F., Clement, A. C., Broccoli, A. J., and Erb, M. P.: Climate feedbacks in  
1881   response to changes in obliquity, *Journal of Climate*, 24, 2830–2845,  
1882   doi:10.1175/2010JCLI3986.1, URL  
1883   <https://journals.ametsoc.org/view/journals/clim/24/11/2010jcli3986.1.xml>, 2011.  
1884  
1885   Marcott, S. A., Bauska, T. K., Buizert, C., Steig, E. J., Rosen, J. L., Cuffey, K. M., Fudge, T.  
1886   J., Severinghaus, J. P., Ahn, J., Kalk, M. L., McConnell, J. R., Sowers, T., Taylor, K.  
1887   C., White, J. W. C., and Brook, E. J.: Centennial-scale changes in the global carbon  
1888   cycle during the last deglaciation, *Nature*, 514, 616–619, doi:10.1038/nature13799,  
1889   URL <https://doi.org/10.1038/nature13799>, 2014.  
1890  
1891   Margari, V., Skinner, L. C., Tzedakis, P. C., Ganopolski, A., Vautravers, M., and Shackleton,  
1892   N. J.: The nature of millennial-scale climate variability during the past two glacial  
1893   periods, *Nature Geoscience*, 3, 127–131, doi:10.1038/ngeo740, URL  
1894   <https://doi.org/10.1038/ngeo740>, 2010.  
1895  
1896   Margari, V., Skinner, L., Hodell, D., Martrat, B., Toucanne, S., Gibbard, P., Lunkka, J., and  
1897   Tzedakis, C.: Land-ocean changes on orbital and millennial time scales and the  
1898   penultimate glaciation, *Geology*, doi:10.1130/G35070.1, 2014.  
1899  
1900   Margari, V., Skinner, L. C., Menviel, L., Capron, E., Rhodes, R. H., Mleneck-Vautravers, M.  
1901   J., Ezat, M. M., Martrat, B., Grimalt, J. O., Hodell, D. A., and Tzedakis, P. C.: Fast  
1902   and slow components of interstadial warming in the North Atlantic during the last  
1903   glacial, *Communications Earth & Environment*, 1, 6, doi:10.1038/s43247-020-0006-  
1904   x, URL <https://doi.org/10.1038/s43247-020-0006-x>, 2020  
1905  
1906   Marshall, S. J. and Koutnik, M. R.: Ice Sheet Action Versus Reaction: Distinguishing  
1907   between Heinrich Events and Dansgaard-Oeschger Cycles in the North Atlantic,  
1908   *Paleoceanography*, 21, 1–13, 2006.  
1909  
1910   Martinez-Boti, M. A., Foster, G. L., Chalk, T. B., Rohling, E. J., Sexton, P. F., Lunt, D. J.,  
1911   Pancost, R. D., Badger, M. P. S., and Schmidt, D. N.: Plio-Pleistocene climate

1912 sensitivity evaluated using high-resolution CO<sub>2</sub> records, *Nature*, 518, 49–54,  
 1913 doi:10.1038/nature14145, URL <https://doi.org/10.1038/nature14145>, 2015.  
 1914  
 1915 Martrat, B., Grimalt, J. O., Shackleton, N. J., de Abreu, L., Hutterli, M.A., and Stocker, T.  
 1916 F.: Four climate cycles of recurring deep and surface water destabilizations on the  
 1917 Iberian Margin, *Science*, 317, 502–507, doi:10.1126/science.1139994, URL  
 1918 <https://www.science.org/doi/abs/10.1126/science.1139994>, 2007.  
 1919  
 1920 McIntyre, K., Delaney, M. L., and Ravelo, A. C.: Millennial-scale climate change and  
 1921 oceanic processes in the Late Pliocene and Early Pleistocene, *Paleoceanography*, 16,  
 1922 535–543, doi:<https://doi.org/10.1029/2000PA000526>, URL  
 1923 <https://agupubs.onlinelibrary.wiley.com/doi/abs/10.1029/2000PA000526>, 2001.  
 1924  
 1925 McManus, J. F., Oppo, D. W., and Cullen, J. L.: A 0.5-million-year record of millennial-scale  
 1926 climate variability in the North Atlantic, *Science*, 283, 971–975,  
 1927 doi:10.1126/science.283.5404.971, URL  
 1928 <https://www.science.org/doi/abs/10.1126/science.283.5404.971>, 1999.  
 1929  
 1930 McManus, J. F., Francois, R., Gherardi, J. M., Keigwin, L. D., and Brown-Leger, S.:  
 1931 Collapse and rapid resumption of Atlantic meridional circulation linked to deglacial  
 1932 climate changes, *Nature*, 428, 834–837, doi: 10.1038/nature02494, URL  
 1933 <https://doi.org/10.1038/nature02494>, 2004.  
 1934  
 1935 Menviel, L. C., Skinner, L. C., Tarasov, L., and Tzedakis, P. C.: An ice–climate oscillatory  
 1936 framework for Dansgaard–Oeschger cycles, *Nature Reviews Earth and Environment*,  
 1937 1, 677–693, doi:10.1038/s43017-020-00106-y, URL [https://doi.org/10.1038/s43017-](https://doi.org/10.1038/s43017-020-00106-y)  
 1938 [020-00106-y](https://doi.org/10.1038/s43017-020-00106-y), 2020.  
 1939  
 1940 [Mukhin, D., Gavrilov, A., Loskutov, E., Kurths, J., and Feigin, A.: Bayesian data analysis for](#)  
 1941 [revealing causes of the Middle Pleistocene Transition, \*Scientific Reports\*, 9, 7328,](#)  
 1942 <https://doi.org/10.1038/s41598-019-43867-3>, 2019.  
 1943  
 1944 Nehrbass-Ahles, C., Shin, J., Schmitt, J., Bereiter, B., Joos, F., Schilt, A., Schmidely, L.,  
 1945 Silva, L., Teste, G., Grilli, R., Chappellaz, J., Hodell, D., Fischer, H., and Stocker,  
 1946 T. F.: Abrupt CO<sub>2</sub> release to the atmosphere under glacial and early interglacial  
 1947 climate conditions, *Science*, 369, 1000–1005, doi:10.1126/science.aay8178, URL  
 1948 <https://www.science.org/doi/abs/10.1126/science.aay8178>, 2020.  
 1949  
 1950 Niu, L., Lohmann, G., and Gowan, E. J.: Climate noise influences ice sheet mean state,  
 1951 *Geophysical Research Letters*, 46, 9690–9699,  
 1952 doi:<https://doi.org/10.1029/2019GL083717>, URL  
 1953 <https://agupubs.onlinelibrary.wiley.com/doi/abs/10.1029/2019GL083717>, 2019.  
 1954  
 1955 North Greenland Ice Core Project Members: High-resolution record of Northern Hemisphere  
 1956 climate extending into the last interglacial period, *Nature*, 431, 147–151,  
 1957 doi:10.1038/nature02805, URL <https://doi.org/10.1038/nature02805>, 2004.  
 1958  
 1959 Oliveira, D., Desprat, S., Rodrigues, T., Naughton, F., Hodell, D., Trigo, R., Rufino, M.,  
 1960 Lopes, C., Abrantes, F., and Sanchez Goni, M.: The complexity of millennial-scale

Formatted: Font: 12 pt, Font colour: Text 1

Formatted: Font: 12 pt, Font colour: Text 1

Formatted: Font: 12 pt, Font colour: Text 1

Formatted: Font: 12 pt, Font colour: Text 1

Formatted: Font: (Default) Times New Roman, 12 pt, Font colour: Text 1



1961 variability in southwestern Europe during MIS 11, *Quaternary Research*, 86,  
1962 doi:10.1016/j.yqres.2016.09.002, 2016.  
1963  
1964 Oliveira, D., Sanchez Goni, M. F., Naughton, F., Polanco-Martinez, J., Jimenez-Espejo,  
1965 F. J., Grimalt, J. O., Martrat, B., Voelker, A. H., Trigo, R., Hodell, D., Abrantes, F.,  
1966 and Desprat, S.: Unexpected weak seasonal climate in the western Mediterranean  
1967 region during MIS 31, a high-insolation forced interglacial, *Quaternary Science*  
1968 *Reviews*, 161, 1–17, doi:<https://doi.org/10.1016/j.quascirev.2017.02.013>, URL  
1969 <https://www.sciencedirect.com/science/article/pii/S0277379116306515>, 2017.  
1970  
1971 Oppo, D. W., McManus, J. F., and Cullen, J. L.: Abrupt climate events 500,000 to 340,000  
1972 years ago: Evidence from subpolar North Atlantic sediments, *Science*, 279, 1335–  
1973 1338, doi:10.1126/science.279.5355.1335, URL  
1974 <https://www.science.org/doi/abs/10.1126/science.279.5355.1335>, 1998.  
1975  
1976 [Pälike, H., Norris, R.D., Herrle, J.O., Wilson, P.A., Coxall, H., Lear, C.H., Shackleton, N.J.,](#)  
1977 [Tripathi, A.K., and Wade, B.S.: The Heartbeat of the Oligocene Climate System.](#)  
1978 [Science](#), 314(5807), 1894–1898, <https://doi.org/10.1126/science.1133822>, 2006.  
1979  
1980 Pena, L. D. and Goldstein, S. L.: Thermohaline circulation crisis and impacts during the mid-  
1981 Pleistocene transition, *Science*, 345, 318–322, doi:10.1126/science.1249770, URL  
1982 <https://www.science.org/doi/abs/10.1126/science.1249770>, 2014.  
1983  
1984 Petersen, S.V., Schrag, D. P., and Clark, P. U.: A new mechanism for Dansgaard-Oeschger  
1985 cycles, *Paleoceanography*, 28, 24–30, doi:<https://doi.org/10.1029/2012PA002364>,  
1986 URL <https://agupubs.onlinelibrary.wiley.com/doi/abs/10.1029/2012PA002364>, 2013.  
1987  
1988 Pol, K., Masson-Delmotte, V., Johnsen, S., Bigler, M., Cattani, O., Durand, G., Falourd, S.,  
1989 Jouzel, J., Minster, B., Parrenin, F., Ritz, C., Steen-Larsen, H., and Stenni, B.: New  
1990 MIS 19 EPICA Dome C high resolution deuterium data: Hints for a problematic  
1991 preservation of climate variability at sub-millennial scale in the “oldest ice”, *Earth*  
1992 *and Planetary Science Letters*, 298, doi:10.1016/J.EPSL.2010.07.030, 2010.  
1993  
1994 Poppelmeier, F., Scheen, J., Jeltsch-Thommes, A., and Stocker, T. F.: Simulated stability of  
1995 the Atlantic Meridional Overturning Circulation during the Last Glacial Maximum,  
1996 *Climate of the Past*, 17, 615–632, doi:10.5194/cp-17-615-2021, URL  
1997 <https://cp.copernicus.org/articles/17/615/2021/>, 2021.  
1998  
1999 Primeau, F. and Deleersnijder, E.: On the time to tracer equilibrium in the global  
2000 ocean, *Ocean Science*, 5, 13–28, doi:10.5194/os-5-13-2009, URL  
2001 <https://os.copernicus.org/articles/5/13/2009/>, 2009.  
2002  
2003 Rahmstorf, S., Crucifix, M., Ganopolski, A., Goosse, H., Kamenkovich, I., Knutti, R.,  
2004 Lohmann, G., Marsh, R., Mysak, L., Wang, Z., and Weaver, A.: Thermohaline  
2005 circulation hysteresis: A model intercom- parison, *Geophysical Research Letters*, 322,  
2006 doi:10.1029/2005GL023655, 2005.  
2007  
2008 Railsback, L., Gibbard, P., Head, M., Voarintsoa, N. R., and Toucanne, S.: An optimized  
2009 scheme of lettered marine isotope substages for the last 1.0 million years, and

Deleted: ¶

¶ Pailler, D. and Bard, E.: High frequency palaeoceanographic changes during the past 140000 yr recorded by the organic matter in sediments of the Iberian Margin, *Palaeogeography, Palaeoclimatology, Palaeoecology*, 181, 431–452, doi:[https://doi.org/10.1016/S0031-0182\(01\)00444-8](https://doi.org/10.1016/S0031-0182(01)00444-8), URL <https://www.sciencedirect.com/science/article/pii/S0031018201004448>, 2002¶

- 2022 the climatostratigraphic nature of isotope stages and substages, *Quaternary Science*  
 2023 *Reviews*, 111, 94–106, doi:10.1016/j.quascirev.2015.01.012, 2015.
- 2024
- 2025 Raymo, M., Ganley, K., Carter, S., Oppo, D., and McManus, J.: Millennial-scale instability  
 2026 during the early Pleistocene epoch, *Nature*, 392, 699–702, doi:10.1038/33658, 1998.
- 2027
- 2028 Raymo, M. E.: The timing of major climate terminations, *Paleoceanography*, 12, 577–585,  
 2029 doi:<https://doi.org/10.1029/97PA01169>, URL  
 2030 <https://agupubs.onlinelibrary.wiley.com/doi/abs/10.1029/97PA01169>, 1997.
- 2031
- 2032 Raymo, M. E. and Nisancioglu, K. H.: The 41 kyr world: Milankovitch's other unsolved  
 2033 mystery, *Paleoceanography*, 18, doi:<https://doi.org/10.1029/2002PA000791>, URL  
 2034 <https://agupubs.onlinelibrary.wiley.com/doi/abs/10.1029/2002PA000791>, 2003.
- 2035
- 2036 Raymo, M. E., Oppo, D. W., and Curry, W.: The Mid-Pleistocene climate transition: A  
 2037 deep sea carbon isotopic perspective, *Paleoceanography*, 12, 546–559,  
 2038 doi:<https://doi.org/10.1029/97PA01019>, URL  
 2039 <https://agupubs.onlinelibrary.wiley.com/doi/abs/10.1029/97PA01019>, 1997.
- 2040
- 2041 Rhines, A. and Huybers, P.: Estimation of spectral power laws in time uncertain series of data  
 2042 with application to the Greenland Ice Sheet Project  $\delta^{18}\text{O}$  record, *Journal of*  
 2043 *Geophysical Research: Atmospheres*, 116, doi:<https://doi.org/10.1029/2010JD014764>,  
 2044 URL <https://agupubs.onlinelibrary.wiley.com/doi/abs/10.1029/2010JD014764>, 2011.
- 2045
- 2046 Rodrigues, T., Alonso-García, M., Hodell, D., Rufino, M., Naughton, F., Grimalt, J.,  
 2047 Voelker, A., and Abrantes, F.: A 1-Ma record of sea surface temperature and extreme  
 2048 cooling events in the North Atlantic: A perspective from the Iberian Margin,  
 2049 *Quaternary Science Reviews*, 172, 118–130,  
 2050 doi:<https://doi.org/10.1016/j.quascirev.2017.07.004>, URL  
 2051 <https://www.sciencedirect.com/science/article/pii/S027737911630590X>, 2017.
- 2052
- 2053 Sakai, K. and Peltier, W. R.: A dynamical systems model of the Dansgaard–Oeschger  
 2054 oscillation and the origin of the Bond Cycle, *Journal of Climate*, 12, 2238–2255,  
 2055 doi:10.1175/1520-0442, URL  
 2056 <https://journals.ametsoc.org/view/journals/clim/12/8/1520-044219990122238adsmot2>
- 2057
- 2058 Sanchez Goni, M., Rodrigues, T., Hodell, D., Polanco-Martinez, J., Alonso-Garcia, M.,  
 2059 Hernandez-Almeida, I., Desprat, S., and Ferretti, P.: Tropically-driven climate  
 2060 shifts in southwestern Europe during MIS 19, a low eccentricity interglacial, *Earth*  
 2061 *and Planetary Science Letters*, 448, 81–93,  
 2062 doi:<https://doi.org/10.1016/j.epsl.2016.05.018>, URL  
 2063 <https://www.sciencedirect.com/science/article/pii/S0012821X16302357>, 2016.
- 2064
- 2065 Sevellec, F. and Fedorov, A. V.: Unstable AMOC during glacial intervals and millennial  
 2066 variability: The role of mean sea ice extent, *Earth and Planetary Science Letters*, 429,  
 2067 60–68, doi:<https://doi.org/10.1016/j.epsl.2015.07.022>, URL  
 2068 <https://www.sciencedirect.com/science/article/pii/S0012821X15004495>, 2015.
- 2069
- 2070 Shackleton, N., Fairbanks, R., Chiu, T., and Parrenin, F.: Absolute calibration of the  
 2071 Greenland time scale: implications for Antarctic time scales and for  $^{14}\text{C}$ , *Quaternary*

2072 Science Reviews, 23, 1513–1522,  
2073 doi:<https://doi.org/10.1016/j.quascirev.2004.03.006>, URL  
2074 <https://www.sciencedirect.com/science/article/pii/S0277379104000824>, 2004.  
2075

2076 Shackleton, N. J., Hall, M. A., and Vincent, E.: Phase relationships between millennial-scale  
2077 events 64,000–24,000 years ago, *Paleoceanography*, 15, 565–569,  
2078 doi:<https://doi.org/10.1029/2000PA000513>, URL  
2079 <https://agupubs.onlinelibrary.wiley.com/doi/abs/10.1029/2000PA000513>, 2000.  
2080

2081 Shin, J., Nehrbass-Ahles, C., Grilli, R., Chowdhry Beeman, J., Parrenin, F., Teste, G.,  
2082 Landais, A., Schmidely, L., Silva, L., Schmitt, J., Bereiter, B., Stocker, T. F., Fischer,  
2083 H., and Chappellaz, J.: Millennial-scale atmospheric CO<sub>2</sub> variations during the  
2084 Marine Isotope Stage 6 period (190–135 ka), *Climate of the Past*, 16, 2203–2219,  
2085 doi:10.5194/cp-16-2203-2020, URL  
2086 <https://cp.copernicus.org/articles/16/2203/2020/>, 2020.  
2087

2088 Siddall, M., Rohling, E. J., Thompson, W. G., and Waelbroeck, C.: Marine isotope stage 3  
2089 sea level fluctuations: Data synthesis and new outlook, *Reviews of Geophysics*, 46,  
2090 doi:<https://doi.org/10.1029/2007RG000226>, URL  
2091 <https://agupubs.onlinelibrary.wiley.com/doi/abs/10.1029/2007RG000226>, 2008.  
2092

2093 Sima, A., Paul, A., and Schulz, M.: The Younger Dryas - An intrinsic feature of late  
2094 Pleistocene climate change at millennial timescales, *Earth and Planetary Science*  
2095 *Letters*, 222, 741–750, doi:10.1016/j.epsl.2004.03.026, 2004.  
2096

2097 Skinner, L. and McCave, I.: Analysis and modeling of gravity and piston coring based on soil  
2098 mechanics, *Marine Geology*, 199, 181–204, doi:10.1016/S0025-3227(03)00127-0,  
2099 2003.  
2100

2101 Skinner, L. and Shackleton, N.: An Atlantic lead over Pacific deep-water change across  
2102 Termination I: implications for the application of the marine isotope stage  
2103 stratigraphy, *Quaternary Science Reviews*, 24, 571–  
2104 580, doi:<https://doi.org/10.1016/j.quascirev.2004.11.008>, URL  
2105 <https://www.sciencedirect.com/science/article/pii/S0277379104003336>,  
2106 2005.  
2107

2108 Skinner, L. and Shackleton, N.: Deconstructing Terminations I and II: Revisiting the  
2109 glacioeustatic paradigm based on deep-water temperature estimates, *Quaternary*  
2110 *Science Reviews*, 25, 3312–3321, doi:10.1016/j.quascirev.2006.07.005, 2006.  
2111

2112 Skinner, L. C., Shackleton, N. J., and Elderfield, H.: Millennial-scale variability of deep-  
2113 water temperature and <sup>18</sup>O<sub>dw</sub> indicating deep-water source variations in the Northeast  
2114 Atlantic, 0–34 cal. ka BP, *Geochemistry, Geophysics, Geosystems*, 4,  
2115 doi:<https://doi.org/10.1029/2003GC000585>, URL  
2116 <https://agupubs.onlinelibrary.wiley.com/doi/abs/10.1029/2003GC000585>, 2003.  
2117

2118 Skinner, L. C., Elderfield, H., and Hall, M.: Phasing of millennial climate events and  
2119 northeast Atlantic Deep-Water temperature change since 50 Ka BP, pp. 197–208,  
2120 American Geophysical Union (AGU), doi:<https://doi.org/10.1029/173GM14>, URL  
2121 <https://agupubs.onlinelibrary.wiley.com/doi/abs/10.1029/173GM14>, 2007.

2122 Skinner, L. C., Fallon, S., Waelbroeck, C., Michel, E., and Barker, S.: Ventilation of the deep  
2123 Southern Ocean and deglacial CO<sub>2</sub> rise, *Science*, 328, 1147–  
2124 1151, doi:10.1126/science.1183627, URL  
2125 <https://www.science.org/doi/abs/10.1126/science.1183627>, 2010.  
2126  
2127  
2128 Skinner, L., Menviel, L., Broadfield, L., Gottschalk, J., and Greaves,  
2129 M.: Southern Ocean convection amplified past Antarctic warming  
2130 and atmospheric CO<sub>2</sub> rise during Heinrich Stadial 4, *Communications*  
2131 *Earth & Environment*, 1, 23, doi:10.1038/s43247-020-00024-3, URL  
2132 <https://doi.org/10.1038/s43247-020-00024-3>, 2020.  
2133  
2134 Stocker, T. F.: The Seesaw Effect, *Science*, 282, 61–62, doi:10.1126/science.282.5386.61,  
2135 URL <https://www.science.org/doi/abs/10.1126/science.282.5386.61>, 1998.  
2136  
2137 Stocker, T. F. and Johnsen, S. J.: A minimum thermodynamic model for the bipolar seesaw,  
2138 *Paleoceanography*, 18, doi:<https://doi.org/10.1029/2003PA000920>, URL  
2139 <https://agupubs.onlinelibrary.wiley.com/doi/abs/10.1029/2003PA000920>, 2003.  
2140  
2141 Sun, Y., McManus, J. F., Clemens, S. C., Zhang, X., Vogel, H., Hodell, D. A., Guo, F.,  
2142 Wang, T., Liu, X., and An, Z.: Persistent orbital influence on millennial climate  
2143 variability through the Pleistocene, *Nature Geoscience*, 14, 812–818,  
2144 doi:10.1038/s41561-021-00794-1, URL <https://doi.org/10.1038/s41561-021-00794-1>,  
2145 2021.  
2146  
2147 Thomas, N.C., Bradbury, H.J., and Hodell, D.A.: Changes in North Atlantic deep-water  
2148 oxygenation across the Middle Pleistocene Transition, *Science*,  
2149 [science.org/doi/10.1126/science.abj7761](https://doi.org/10.1126/science.abj7761), 2022.  
2150  
2151 Timmermann, A., Gildor, H., Schulz, M., and Tziperman, E.: Coherent resonant millennial-  
2152 scale climate oscillations triggered by massive meltwater pulses, *Journal of Climate*,  
2153 16, 2569 – 2585, doi:10.1175/1520-0442, URL  
2154 <https://journals.ametsoc.org/view/journals/clim/16/15/1520-044220030162569crmcot>,  
2155 2003.  
2156  
2157 Tuenter, E., Weber, S. L., Hilgen, F. J., and Lourens, L. J.: Sea-ice feedbacks on  
2158 the climatic response to precession and obliquity forcing, *Geophysical*  
2159 *Research Letters*, 32, doi:<https://doi.org/10.1029/2005GL024122>, URL  
2160 <https://agupubs.onlinelibrary.wiley.com/doi/abs/10.1029/2005GL024122>,  
2161 2005.  
2162  
2163 Tzedakis, P., Margari, V., and Hodell, D.: Coupled ocean–land millennial-scale changes  
2164 1.26 million years ago, recorded at Site U1385 off Portugal, *Global and Planetary*  
2165 *Change*, 135, 83– 88, doi:<https://doi.org/10.1016/j.gloplacha.2015.10.008>, URL  
2166 <https://www.sciencedirect.com/science/article/pii/S0921818115300850>, 2015.  
2167  
2168 Tzedakis, P. C., Drysdale, R. N., Margari, V., Skinner, L. C., Menviel, L., Rhodes, R. H.,  
2169 Taschetto, A. S., Hodell, D. A., Crowhurst, S. J., Hellstrom, J. C., Fallick, A.  
2170 E., Grimalt, J. O., McManus, J. F., Martrat, B., Mokeddem, Z., Parrenin, F.,  
2171 Regattieri, E., Roe, K., and Zanchetta, G.: Enhanced climate instability in the North

2172 Atlantic and southern Europe during the Last Interglacial, *Nature Communications*, 9,  
2173 4235, doi:10.1038/s41467-018-06683-3, URL [https://doi.org/10.1038/s41467-018-](https://doi.org/10.1038/s41467-018-06683-3)  
2174 06683-3, 2018.  
2175

2176 Vautravers, M. J. and Shackleton, N. J.: Centennial-scale surface hydrology off Portugal  
2177 during marine isotope stage 3: Insights from planktonic foraminiferal fauna  
2178 variability, *Paleoceanography*, 21, doi:<https://doi.org/10.1029/2005PA001144>, URL  
2179 <https://agupubs.onlinelibrary.wiley.com/doi/abs/10.1029/2005PA001144>, 2006.  
2180

2181 Verbitsky, M. Y., Crucifix, M., and Volobuev, D. M.: A theory of Pleistocene glacial  
2182 rhythmicity, *Earth System Dynamics*, 9, 1025–1043, doi:10.5194/esd-9-1025-2018,  
2183 URL <https://esd.copernicus.org/articles/9/1025/2018/>, 2018.  
2184

2185 Vettoretti, G., Ditlevsen, P., Jochum, M., and Rasmussen, S. O.: Atmospheric CO<sub>2</sub> control of  
2186 spontaneous millennial-scale ice age climate oscillations, *Nature Geoscience*, 15,  
2187 300–306, doi:10.1038/s41561-022-00920-7, URL [https://doi.org/10.1038/s41561-](https://doi.org/10.1038/s41561-022-00920-7)  
2188 022-00920-7, 2022.  
2189

2190 Vimeux, F., Masson, V., Jouzel, J., Stievenard, M., and Petit, J. R.: Glacial–interglacial  
2191 changes in ocean surface conditions in the Southern Hemisphere, *Nature*, 398, 410–  
2192 413, doi:10.1038/18860, URL <https://doi.org/10.1038/18860>, 1999.  
2193

2194 Waelbroeck, C., Skinner, L. C., Labeyrie, L., Duplessy, J.-C., Michel, E., Vazquez Riveiros,  
2195 N., Gherardi, J.-M., and Dewilde, F.: The timing of deglacial circulation changes in  
2196 the Atlantic, *Paleoceanography*, 26, doi:<https://doi.org/10.1029/2010PA002007>, URL  
2197 <https://agupubs.onlinelibrary.wiley.com/doi/abs/10.1029/2010PA002007>,  
2198 2011  
2199

2200

2201 WAIS Divide Project Members: Precise inter-polar phasing of abrupt climate change during  
2202 the last ice age, *Nature*, 520, 661–665, doi:10.1038/nature14401, URL  
2203 <https://doi.org/10.1038/nature14401>, 2015.  
2204

2205 Weirauch, D., Billups, K., and Martin, P.: Evolution of millennial-scale climate variability  
2206 during the mid-Pleistocene, *Paleoceanography*, 23,  
2207 doi:<https://doi.org/10.1029/2007PA001584>, URL  
2208 <https://agupubs.onlinelibrary.wiley.com/doi/abs/10.1029/2007PA001584>, 2008.  
2209

2210 Winton, M. and Sarachik, E. S.: Thermohaline oscillations induced by strong steady salinity  
2211 forcing of ocean general circulation models, *Journal of Physical Oceanography*, 23,  
2212 1389–1410, doi:10.1175/1520-0485, URL  
2213 [https://journals.ametsoc.org/view/journals/phoc/23/7/1520-](https://journals.ametsoc.org/view/journals/phoc/23/7/1520-048519930231389toibss20c)  
2214 048519930231389toibss20c  
2215

2216 Wolff, E. W., Fischer, H., and Rothlisberger, R.: Glacial terminations as southern  
2217 warmings without northern control, *Nature Geoscience*, 2, 206–209, doi:  
2218 10.1038/ngeo442, URL <https://doi.org/10.1038/ngeo442>, 2009.  
2219

2220 Wolff, E. W., Fischer, H., van Ommen, T., and Hodell, D. A.: Stratigraphic templates for  
2221 ice core records of the past 1.5 million years, *Climate of the Past Discussions*,

2222 2022, 1–22, doi:10.5194/cp-2022-2, URL [https://cp.copernicus.org/preprints/cp-2022-](https://cp.copernicus.org/preprints/cp-2022-2/)  
2223 2/, 2022.  
2224  
2225 Yan, Y., Bender, M. L., Brook, E. J., Clifford, H. M., Kemeny, P. C., Kurbatov, A. V.,  
2226 Mackay, S., Mayewski, P. A., Ng, J., Severinghaus, J. P., and Higgins, J. A.: Two-  
2227 million-year-old snapshots of atmospheric gases from Antarctic ice, *Nature*, 574,  
2228 663–666, doi:10.1038/s41586-019-1692-3, URL [https://doi.org/10.1038/s41586-019-](https://doi.org/10.1038/s41586-019-1692-3)  
2229 1692-3, 2019.  
2230  
2231 Yin, Q. Z., Wu, Z. P., Berger, A., Gooose, H., and Hodell, D.: Insolation triggered abrupt  
2232 weakening of Atlantic circulation at the end of interglacials, *Science*, 373, 1035–  
2233 1040, doi:10.1126/science.abg1737, URL  
2234 <https://www.science.org/doi/abs/10.1126/science.abg1737>, 2021.  
2235  
2236 Zhang, X., Lohmann, G., Knorr, G., and Purcell, C.: Abrupt glacial climate shifts  
2237 controlled by ice sheet changes, *Nature*, 512, 290–294, doi: 10.1038/nature13592,  
2238 URL <https://doi.org/10.1038/nature13592>, 2014.  
2239  
2240 Zhang, X., Knorr, G., Lohmann, G., and Barker, S.: Abrupt North Atlantic circulation  
2241 changes in response to gradual CO<sub>2</sub> forcing in a glacial climate state, *Nature*  
2242 *Geoscience*, 10, 518–523, doi:10.1038/ngeo2974, URL  
2243 <https://doi.org/10.1038/ngeo2974>, 2017.  
2244  
2245 Zhang, X., Barker, S., Knorr, G., Lohmann, G., Drysdale, R., Sun, Y., Hodell, D., and Chen,  
2246 F.: Direct astronomical influence on abrupt climate variability, *Nature Geoscience*,  
2247 14, 819–826, doi:10.1038/s41561-021-00846-6, URL  
2248 <https://doi.org/10.1038/s41561-021-00846-6>, 2021.  
2249  
2250 Zitellini, N., Gracia, E., Matias, L., Terrinha, P., Abreu, M., DeAlteriis, G., Henriët, J.,  
2251 Danobeitia, J., Masson, D., Mulder, T., Ramella, R., Somoza, L., and Diez, S.: The  
2252 quest for the Africa–Eurasia plate boundary west of the Strait of Gibraltar, *Earth and*  
2253 *Planetary Science Letters*, 280, 13–50, doi:<https://doi.org/10.1016/j.epsl.2008.12.005>,  
2254 URL <https://www.sciencedirect.com/science/article/pii/S0012821X0800753X>, 2009.  
2255

Page 14: [1] Deleted      David A. Hodell      03/01/2023 14:08:00

Page 14: [2] Deleted      David A. Hodell      03/01/2023 14:08:00